RESEARCH ARTICLE

Key Points:

- Ash deposition triggers phytoplankton blooms at Nishinoshima during the explosive phase of the 2019–2020 eruption
- Phytoplankton blooms were not present during the effusive phase of the 2019–2020 eruption
- Phytoplankton blooms triggered by ash deposition can lead to carbon drawdown that can mediate the carbon output from the eruption

Ash Deposition Triggers Phytoplankton Blooms at Nishinoshima Volcano, Japan

Liam J. Kelly[1] , **Kristen E. Fauria[1]** , **Tushar Mittal[2]**, **Jan El Kassar[3]** , **Ralf Bennartz[1]** , **David Nicholson[4]** , **Ajit Subramaniam[5]** , and **Ashok Kumar Gupta[6]**

[1]Department of Earth and Environmental Sciences, Vanderbilt University, Nashville, TN, USA, [2]Department of Geosciences, The Pennsylvania State University, State College, PA, USA, [3]Department of Geosciences, Institute of Meteorology, WG Radiation & Remote Sensing, Freie Universität Berlin, Berlin, Germany, [4]Department of Marine Chemistry and Geochemistry, Woods Hole Oceanographic Institution, Woods Hole, MA, USA, [5]Lamont-Doherty Earth Observatory, Columbia University, Palisades, NY, USA, [6]Department of Atmospheric and Oceanic Sciences, University of California, Los Angeles, Los Angeles, CA, USA

Abstract Volcanoes that deposit eruptive products into the ocean can trigger phytoplankton blooms near the deposition area. Phytoplankton blooms impact the global carbon cycle, but the specific conditions and mechanisms that facilitate volcanically triggered blooms are not well understood, especially in low nutrient ocean regions. We use satellite remote sensing to analyze the chlorophyll response to an 8-month period of explosive and effusive activity from Nishinoshima volcano, Japan. Nishinoshima is an ocean island volcano in a low nutrient low chlorophyll region of the Northern Pacific Ocean. From June to August 2020, during explosive activity, satellite-derived chlorophyll-*a* was detectable with amplitudes significantly above the long-term climatological value. After the explosive activity ceased in mid-August 2020, these areas of heightened chlorophyll concentration decreased as well. In addition, we used aerial observations and satellite imagery to demonstrate a spatial correlation between blooms and ash plume direction. Using a sun-induced chlorophyll-*a* fluorescence satellite product, we confirmed that the observed chlorophyll blooms are phytoplankton blooms. Based on an understanding of the nutrients needed to supply blooms, we hypothesize that blooms of nitrogen-fixing phytoplankton led to a 10^{10}–10^{12} g drawdown of carbon. Thus, the bloom could have significantly mediated the output of carbon from the explosive phase of the eruption but is a small fraction of anthropogenic CO_2 stored in the ocean or the global biological pump. Overall, we provide a case study of fertilization of a nutrient-poor ocean with volcanic ash and demonstrate a scenario where multi-month scale deposition triggers continuous phytoplankton blooms across 1,000s of km^2.

Plain Language Summary Volcanic eruptions can cause organisms known as phytoplankton to multiply and form what is known as a phytoplankton bloom in the ocean. Phytoplankton blooms can impact the life cycle of carbon in the earth system, but it is not always obvious why phytoplankton blooms happen. Using different satellite data, we observe phytoplankton blooms by viewing chlorophyll concentration in the ocean. Nishinoshima is a remote volcano in an area of the Pacific that lacks nutrients necessary for phytoplankton blooms. Nishinoshima erupted in 2019–2020 and deposited lava and ash into the ocean at different times. By looking at the chlorophyll concentration during the time periods lava and ash were deposited into the ocean, we found that chlorophyll concentration increased when ash was deposited into the ocean. These increases in chlorophyll concentration were determined to be phytoplankton blooms. These phytoplankton blooms may utilize nutrients from volcanic ash and the atmosphere, leading to a drawdown of atmospheric carbon.

1. Introduction

Volcanoes have important impacts on many large-scale earth system processes, including stimulating phytoplankton blooms. Phytoplankton blooms matter because they are a key component of the biological pump in the global carbon cycle. Blooms have been associated with several different volcanic eruptions such as the 2008 eruptions of Kasatochi, Alaska (Langmann et al., 2010; Lindenthal et al., 2013; Westberry et al., 2019), Okmok, Alaska (Langmann et al., 2010; Westberry et al., 2019), 2018 Kilauea, Hawaii (Wilson et al., 2019), 2001–2007 eruptions at Mount Etna, Italy (Olgun et al., 2013), and 2007 Piton de la Fournaise (Reunion, see Black et al., 2021). However, there are also more cases where eruptions do not lead to significant phytoplankton blooms (Browning et al., 2015). The complicated relationship between volcanism and phytoplankton blooms

indicates that key aspects of bloom triggering are not fully understood. By studying the conditions that facilitate eruption-driven phytoplankton blooms, we can better understand the impact of volcanism on ocean productivity and the global carbon cycle, both in the present and in the paleo-environmental records (Basu & Mackey, 2018; Blain et al., 2007; Lee et al., 2018; Smetacek et al., 2012).

Phytoplankton blooms occur when a limiting nutrient (such as nitrogen, phosphorus, or iron) is added to the system to enable the use of non-limiting nutrients by populations of phytoplankton (Martin & Fitzwater, 1988; Mills et al., 2004; Pulido-Villena et al., 2010; Zhang et al., 2019). Phytoplankton blooms can occur due to the deposition of dust into the ocean (Zhang et al., 2019). In general, phytoplankton blooms sequester CO_2 and impact the carbon cycle by sinking biomass into the deep ocean (Huppert et al., 2002).

Volcanic ash may stimulate phytoplankton blooms in the same way as dust but is far less studied. In addition, previous work has demonstrated two different mechanisms for the volcanic triggering of phytoplankton blooms: (1) the delivery of iron through the deposition of ash in iron-limited regions (Langmann et al., 2010; Lindenthal et al., 2013; Westberry et al., 2019) or (2) the deposition of lava into the ocean resulting in upwelling of deeper, nitrate-rich water (Wilson et al., 2019). These two mechanisms can be associated with explosive (ash, case 1) and effusive (lava flows, case 2) volcanism, respectively.

The background nutrient state of the ocean is a key factor that can control the response of the ocean to the deposition of volcanic products. The nutrients present in the ocean define what nutrients are needed (and can be supplied by volcanism) to impact the phytoplankton population. There are two end members for ocean biogeochemistry where phytoplankton, and as a result, chlorophyll-*a*, concentrations are low: High Nutrient Low Chlorophyll (HNLC) and Low Nutrient Low Chlorophyll (LNLC, see Figure 1 to see HNLC and LNLC regions). Chlorophyll-*a* is a proxy for phytoplankton because it is the main photosynthetic pigment in phytoplankton (Jakobsen & Markager, 2016). In HNLC regions, the ocean is primarily iron-limited, which means nutrients like nitrates and phosphates needed to fuel photosynthesis in phytoplankton are in excess (Martin & Fitzwater, 1988). Iron allows for the increased use of those already present macronutrients (Martin & Fitzwater, 1988). Delivery of iron to an HNLC is thought to be the cause for the 2008 phytoplankton bloom after the eruptions of Kasatochi and Okmok (Langmann et al., 2010; Lindenthal et al., 2013; Westberry et al., 2019).

LNLC regions, which correspond with subtropical ocean gyres, have low concentrations of nitrates, phosphates, and iron. The combination of nutrients delivered to the system must be sufficiently enriched in N, P, and Fe to facilitate phytoplankton blooms (Mills et al., 2004; Pulido-Villena et al., 2010; Zhang et al., 2019). To date, only a handful of studies have examined chlorophyll responses in LNLC regions. The Kilauea 2018 eruption introduced lava into an LNLC region. This lava deposition spurred the upwelling of deep nitrate-rich water that fueled a phytoplankton bloom (Wilson et al., 2019). The 2003 eruption of Anatahan, Mariana Islands deposited volcanic ash in an LNLC region. Lin et al. (2011) used remote sensing to conclude that Anatahan triggered a phytoplankton bloom by increasing nitrogen fixation due to the delivery of iron and phosphorus to the water (Lin et al., 2011). Although this was one of the first studies of a volcanic chlorophyll response in an LNLC region, the Anatahan eruption and corresponding bloom lasted only 1 week. The Etna 2002 eruption also deposited volcanic ash in an LNLC region, which caused phytoplankton growth (Olgun et al., 2013). As illustrated in Figure 1, LNLC regions constitute most of the Earth's oceans and represent regions with typically low productivity. A better understanding of volcanic chlorophyll responses in LNLC regions can improve the extrapolation of the effect of volcanic eruptions and eruption style on ocean biogeochemistry globally.

In this study, we analyzed 8 months of eruptive activity at Nishinoshima Volcano, Japan to better understand the relationship between volcanic eruptions and phytoplankton blooms. Nishinoshima is a remote, ocean island volcano, located in an LNLC region. It has exhibited effusive and explosive eruptions in the past. The 2019–2020 eruption sequence began with effusive eruptions in December 2019 and then transitioned to dominantly explosive eruptions by June 2020 (Figure 2; Kaneko et al. (2022)). This makes Nishinoshima a great case study to address our research questions: (1) Is there a phytoplankton bloom associated with the 2019–2020 eruptions at Nishinoshima? (2) Do phytoplankton blooms occur during the effusive or explosive phase of the eruptive activity? and (3) What are possible mechanisms of the creation of these phytoplankton blooms in an LNLC region?

Due to Nishinoshima's remote location, in situ measurements are difficult. Therefore, we utilize satellite remote sensing methods as our primary means of investigation. This includes the analysis of Synthetic Aperture Radar (SAR) images, Ash/SO_2 red-green-blue (RGB) images, as well as chlorophyll-*a* (Chl_{Sat} and $Chl_{SatMODIS}$), particulate
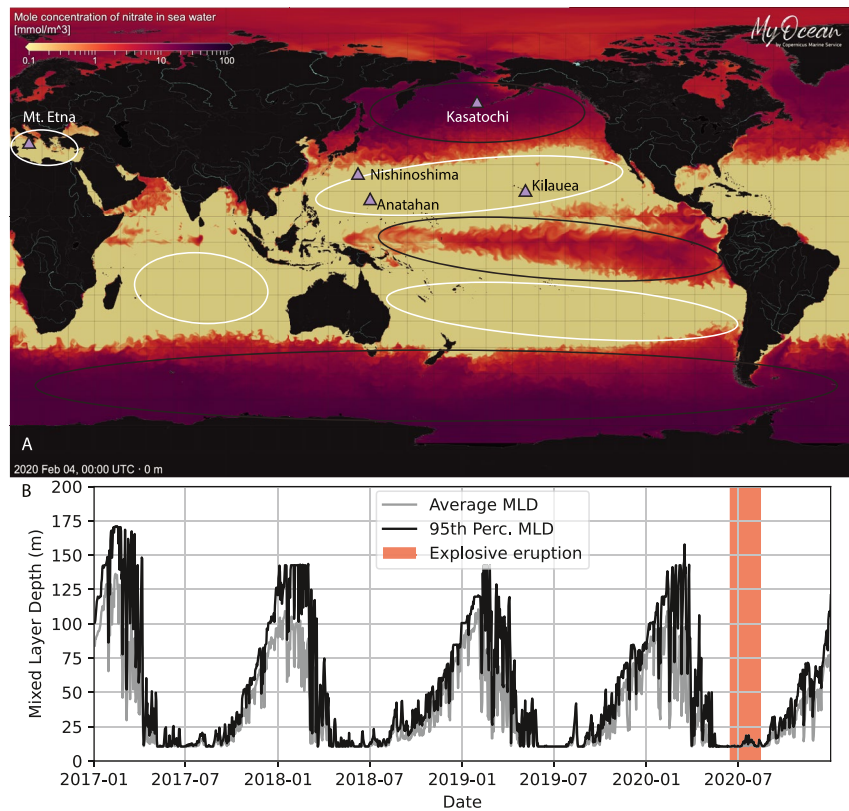
Figure 1. Oceanographic background around Nishinoshima. (a) Map showing LNLC (white circles) and HNLC (black circles) areas throughout the world. Volcanoes of interest with studies of eruption-driven phytoplankton blooms are indicated by purple triangles. This figure shows the concentration of nitrate, whose pattern is also followed by phosphate. The image was taken from CMEMS Global Ocean Biogeochemistry Analysis and Forecast/Hindcast Data sets (E.U. Copernicus Marine Service Information (CMEMS). Marine Data Store (MDS), 2018a, 2019). (b) Time series of Mixed Layer Depth in the ocean around Nishinoshima. During the explosive eruption, displayed by the red box, Mixed Layer depths were between 10 and 20 m. Data supporting this figure from CMEMS Global Ocean Physics Reanalysis (E.U. Copernicus Marine Service Information (CMEMS). Marine Data Store (MDS), 2018b).

organic carbon (POC_{Sat}), and sun-induced fluorescence (F_{Sat}) products. One of the challenges of utilizing chlorophyll and POC_{Sat} products to analyze the biogeochemical state of the ocean is that one cannot always distinguish chlorophyll concentration from discolored water (Komick et al., 2009; Moutzouris-Sidiris & Topouzelis, 2021).
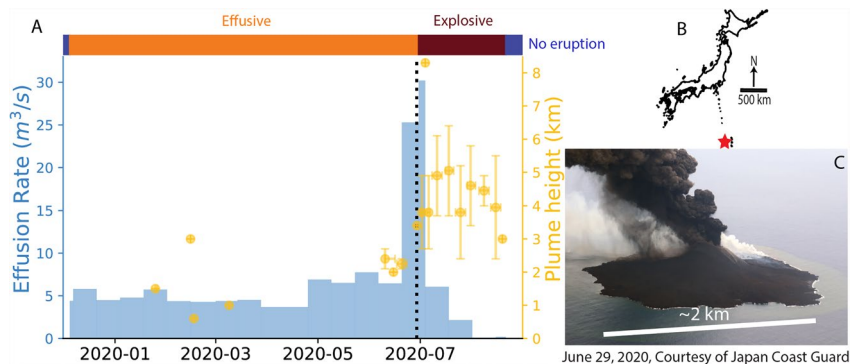
Figure 2. Eruptive history of Nishinoshima. (a) Plot showing effusion rate over the 2019–2020 eruption, taken from Episode 4 paper by Kaneko et al. (2022), and Plume height (Global Volcanism Program, 2020) throughout the 2019–2020 eruption of Nishinoshima. The Black dashed line shows the time of the image of Nishinoshima (c), on 29 June 2020 (Japan Coast Guard, 2020).

Table 1
Satellite-Based Analyses

| Analysis type	Application/description	Satellite	Instrument
SAR imagery	Assess deposition directions of Nishinoshima lava	ALOS-2 (DAICHI-2)[a]	PALSAR-2
Ash/SO2 RGB	Assess presence and direction of ash and SO2	Aqua/Terra[b]	MODIS
Chlorophyll concentration (POLYMER algorithm)[c]	Assess discolored water and chlorophyll presence, the direction of both	Sentinel-3A/B[d]	OLCI
Chlorophyll Fluorescence (OC-Fluo algorithm)[e]	Assess chlorophyll fluorescence, biological signature	Sentinel-3A/B[d]	OLCI
POC	Assess particulate organic carbon concentration in the ocean	Aqua/Terra, via Google Earth Engine[f,g]	MODIS
Chlorophyll concentration (MODIS)	Assess chlorophyll concentration, to compare with POC	Aqua/Terra via Google Earth Engine[f,h]	MODIS

[a]Geospatial Information Authority of Japan (2020). [b]MODIS Characterization Support Team (MCST) (2017). [c]Steinmetz et al. (2011). [d]ESA and EUMETSAT (2022). [e]Kritten et al. (2020). [f]Gorelick et al. (2017). [g]NASA Goddard Space Flight Center, Ocean Ecology Laboratory (2022b). [h]NASA Goddard Space Flight Center, Ocean Ecology Laboratory (2022a).

Therefore, we combine many different satellite products to get a more complete picture of the eruption and volcanic impacts on the ocean. Kaneko et al. (2022) analyzed the discolored water signature around Nishinoshima during the 2019–2020 eruptive activity and concluded that the signatures were not associated with immediate ash deposition. Specifically, Kaneko et al. (2022) observed that the water discoloration did not always align with the direction and extent of ash deposition and thus concluded that the deposition of ash was not the cause of the discoloration. Instead, they proposed that the discoloration was a result of SiO_2-Fe_2O_3-Al_2O_3-H_2O low-crystalline precipitates from seawater interaction with hydrothermal emissions, as observed on the coast of the Izu-Oshima volcano after eruption in 1986 (Ossaka et al., 2000). In contrast, we analyze the full eruptive sequence to account for some time lag in phytoplankton response to ash deposition, which is typically 2–5 days (Browning et al., 2015). During the time-lag, we assume that deposited ash and phytoplankton can be advected by ocean currents such that ash plumes and phytoplankton blooms may not completely align in time and space. By providing a thorough case-study of a volcanically triggered phytoplankton bloom, our study helps to address big picture questions about the feedbacks between volcanism, ocean primary productivity, and climate.

1.1. Geologic/Oceanographic Background

Nishinoshima is an ocean island volcano approximately 1,000 km south of Tokyo, in the Ogasawara Islands of the Izu-Ogasawara Arc (Shinohara et al., 2017) (Figure 2b). It erupted andesitic lava of ~59 wt % SiO_2 (Earthquake Research Institute, 2020; Maeno et al., 2018) in 1973–1974 (Ossaka, 1974) and created a ~0.2 km² island (Tamura et al., 2019). Submarine eruptions began again in November 2013 only 500 m south of the pre-existing island. These eruptions created a new subaerial island that was connected to the existing island by lava flows in late December 2013 (Global Volcanism Program, 2020). Lava flows continued intermittently until 2015 (Global Volcanism Program, 2020) and erupted a total of 8.7×10^7 m³ of andesitic lava (Geospatial Information Authority of Japan, 2016) with a composition of ~59–60 wt % SiO_2 (Earthquake Research Institute, 2020; Maeno et al., 2018). Another eruption occurred in 2017, which was an andesitic effusive eruption (Kaneko et al., 2019) with a composition of ~59 wt % SiO_2 and an average effusion rate of 1.5×10^5 m³/day. In 2019–2020, a series of eruptions took place over 8 months. The 2019–2020 eruptive phase is unique because many months of effusive activity shifted to ash-producing, basaltic andesite explosive eruptions (Global Volcanism Program, 2020) with ash compositions of ~55 wt % SiO_2 (Earthquake Research Institute, 2020; Maeno et al., 2021). Modeling of Advanced Spaceborne Thermal Emission and reflection Radiometer (ASTER) satellite data shows that eruptive plumes exhibit a large portion of fine ash (<25 μm) throughout July 2020 (Williams & Ramsey, 2022). A brief explosive eruptive event in August 2021 (Global Volcanism Program, 2020) is also examined here to provide a comparison to the 2019–2020 eruption.

Nishinoshima is located in a subtropical gyre (Zhang et al., 2019), which are regions that are oligotrophic and low in nutrients and chlorophyll (Lin et al., 2011; Olgun et al., 2013). These LNLC regions are depleted in macronutrients, such as nitrogen and phosphorus, required for the growth of phytoplankton (Lin et al., 2011). As a result, iron may not be the limiting nutrient like it is in HNLC regions (Langmann et al., 2010; Lindenthal et al., 2013). Mixed layer depth in the ocean around Nishinoshima fluctuates throughout the year, with depths as low as 10 m during the summer months (Figure 1b). Since the mixed layer depth and euphotic zone together control the amount of available nutrients and photosynthetically available solar radiation, a shallow mixed layer depth during summer months limits the nutrient supply from below and thereby limits phytoplankton biomass (Diaz et al., 2021; Itoh et al., 2015; Westberry et al., 2023). Thus, shallow mixed layers observed in the summer months around Nishinoshima typically suggest that an external nutrient source, such as volcanic ash, is needed to explain the observed blooms.

2. Methods

We use data from multiple different satellite instruments to assess the temporal and spatial relationships between the 2019–2020 eruptions and the phytoplankton blooms surrounding Nishinoshima Volcano (Table 1). First, we establish the eruption chronology using SAR images captured by the Phased-Array L-band Synthetic Aperture Radar-2 (PALSAR-2) onboard the Advanced Land Observing Satellite-2

(ALOS-2/DAICHI-2) and ash/SO$_2$ RGB images generated from the Moderate Imaging Spectrometer (MODIS) onboard the Terra and Aqua satellites. Then, we examine ocean color observations from MODIS and the Ocean and Land Color Instrument (OLCI) onboard Sentinel 3A and B. For our ocean color investigation, we focus on the timing of water discoloration to understand its relationship to the effusive and explosive phases of the eruption.

2.1. Remote Sensing and Satellite Data

2.1.1. Eruption Chronology

To assess periods of lava versus ash deposition, we reference images generated by the Geospatial Information Authority of Japan using the Japanese Aerospace Exploration Authority satellite ALOS-2 (DAICHI-2) with its onboard SAR instrument (Geospatial Information Authority of Japan, 2020; Yanagisawa et al., 2020). Images from this instrument, taken every 2 weeks, show changes in island morphology and pixel intensity due to ash and lava deposition (Figure S1 in Supporting Information S1). The differences in SAR images are used to determine whether the eruption was primarily effusive, explosive, or a combination, and the general emplacement directions of lava. Comparison of images every 2 weeks allows analysis of surface deformation based on the difference in the phase of waves returned from the surface to the satellite (Massonnet & Feigl, 1998; Yanagisawa et al., 2020). The deposition of ash on the island can be identified when low reflection intensity areas are present in this data (see Figure S1 in Supporting Information S1).

To get a synoptic view of where and when ash is deposited around Nishinoshima, we generate Ash/SO$_2$ RGB images using the MODIS instrument aboard NASA's Terra and Aqua satellites. Data were acquired for all orbits that included the area of Nishinoshima (MODIS Characterization Support Team (MCST), 2017), containing all bands with a spatial resolution of 1 km (MODIS bands 20–36). Ash/SO$_2$ RGB images are generated by taking advantage of the spectral characteristics of ash and SO$_2$ and their differences from traditional water vapor/ice clouds (Gray & Bennartz, 2015; Prata, 2009). Pink colors are plumes higher in ash content, green colors are plumes higher in SO$_2$ content, yellow colors show a mix of ash and SO$_2$, and brown colors typically indicate ice-rich clouds. We do not extract quantitative information from the color of the plume, but rather use the color in a qualitative sense to assess the phase (ash, SO$_2$, or water) that dominates the signal. In our data set, for example, the volcanic plumes appear pink, green, or yellow while meteorological clouds appear brown (Figure 6; Figure S6 in Supporting Information S1). To interpret the RGB imagery, we also use the time history and spatial context. That is, most volcanic plumes are located near a vent. For example, a pink, directional cloud over a volcano is an ash plume, but a round brown cloud some distance from the vent is a meteorological cloud. We note that volcanic plumes can be ice-rich and therefore also appear brown, as was the case for the 2022 Hunga eruption, but we do not see evidence for ice-rich clouds at Nishinoshima (Gray & Bennartz, 2015; Gupta et al., 2022; Prata, 2009). Despite limitations, this method remains one of the best ways to detect volcanic clouds (Prata, 2009). Final images were remapped to ∼2 km resolution. For more details regarding the Ash/SO$_2$ RGB algorithm, see Text S1 in Supporting Information S1 and EUMeTrain (2014).

2.1.2. Ocean Color

We detect phytoplankton blooms in two different ways, through the evaluation of sun-induced fluorescence (F$_{Sat}$) and ocean chlorophyll (Chl$_{Sat}$) products. Both methods use data from the OLCI instrument on the European Space Agency's (ESA) satellite Sentinel-3. Images are available almost daily, and the spatial resolution is 300 m and 1.2 km in full and reduced resolution, respectively (Table 1).

Our first approach for analyzing the discolored water seen around Nishinoshima assesses the chlorophyll concentrations (Chl$_{Sat}$) from OLCI. The OLCI data were processed with the atmospheric correction (AC) algorithm POLYMER (Steinmetz et al., 2011). Chl$_{Sat}$ is used because Chlorophyll-*a* is an indicator of phytoplankton biomass (Morel & Prieur, 1977). Remote sensing products designed to identify chlorophyll should be interpreted with caution, however, because the scattering of light by particles in water means that discolored water from volcanic products in the water column can be misidentified as chlorophyll-rich water (Loisel & Morel, 1998). That said, since POLYMER's estimates of chlorophyll rely on a bio-optical water model rather than a semi-analytic blue-green ratio, it is thought of as more robust against mischaracterizations of non-algal particles (Steinmetz et al., 2011).

Our second approach for assessing the presence of phytoplankton relies on the fluorescence properties of phytoplankton and is more robust against discolored water mischaracterization. Specifically, we use estimates

Table 2
Non-Satellite-Based Analyses

Analysis type	Description	Data source
Plume height	Ash plume heights reached over the eruption at Nishinoshima	Global Volcanism Program[a]
Eruption Style/Chronology	Descriptions of activity, timetable of eruptive activity	Global Volcanism Program, Episode 4 by Kaneko et al. (2022)[a,b]
Eruption Style/Chronology	Aerial photos from above Nishinoshima	Japan Coast Guard[c]
Ocean nutrient state	Modeled concentrations of ocean nutrients, such as nitrate and phosphate	CMEMS[d]
Ocean physics	Modeled mixed layer depth, ocean currents, etc.	CMEMS[e]
Effusion rate	Estimated rates of effusion over time of Nishinoshima over the 2019–2020 eruption	Episode 4 by Kaneko et al. (2022)[b]

[a]Global Volcanism Program (2020). [b]Kaneko et al. (2022). [c]Japan Coast Guard (2020). [d]E.U. Copernicus Marine Service Information (CMEMS). Marine Data Store (MDS) (2018a, 2019). [e]E.U. Copernicus Marine Service Information (CMEMS). Marine Data Store (MDS) (2018b).

of sun-induced fluorescence retrieved from the water-leaving reflectance spectra generated using the POLYMER AC. For that, we apply the OC-Fluo algorithm and generate fields of the fluorescence peak height (F_{Sat}), a measure of the amount of sun-induced chlorophyll-*a* fluorescence. Sun-induced fluorescence is thought to be a more reliable indicator for the presence of phytoplankton than Chl_{Sat} alone due to the ability of particulates to scatter light similarly to the pigment. Traditionally, satellite-retrieved fluorescence products have the potential to be impacted by non-phytoplankton particles present in the water, but the OC-Fluo algorithm is designed to take this effect into account (Kritten et al., 2020). See Text S1 in Supporting Information S1 for more details on methodology and visualization. The relationship between fluorescence and chlorophyll-*a* may not be constant over time, but persistent injection may allow for the preservation of the initial relationship.

We additionally use two Level-3 products from MODIS to assess phytoplankton. These are daily data sets available at 4 km resolution. Specifically, we analyzed the MODIS Chlorophyll-*a* ($Chl_{SatMODIS}$) product (NASA Goddard Space Flight Center, Ocean Ecology Laboratory, 2022a) and Particulate Organic Carbon (POC_{Sat}) product (NASA Goddard Space Flight Center, Ocean Ecology Laboratory, 2022b), which were both accessed through Google Earth Engine. Google Earth Engine is a platform freely available for research, education, and nonprofit use that enables the visualization and analysis of a wide range of geospatial data sets (Gorelick et al., 2017). These data products allow for the confirmation of Chl_{Sat} results with a chlorophyll-*a* product from a different satellite instrument. Maximum POC_{Sat} and $Chl_{SatMODIS}$ were acquired from an area of 6,800 km^2 centered around Nishinoshima.

2.1.3. Directionality of Ash Plumes and Discolored Water

To understand where ash was deposited and Chl_{Sat} was heightened, directions of overall ash deposition and maximum Chl_{Sat} concentration are determined by approximating their cardinal direction in degrees (0–360). Ash deposition directions are determined from Ash/SO$_2$ RGB images, and maximum Chl_{Sat} is determined from contour maps of Sentinel-3 OLCI Chl_{Sat} concentrations. Circles signify cloudy images where no ash plumes are visible. Dates with no data signify days where no ash plumes were present or when Chl_{Sat} was not heightened (see Figure 7). We compare the ash and discolored water orientations to ocean current directions, outlined in more detail below.

2.2. Other Data Sources

We use compiled data sources, including histories from Maeno et al. (2021) and Kaneko et al. (2022), and the Global Volcanism Program (GVP), to create a timeline of the 2019–2020 eruption of Nishinoshima (Table 2). The Global Volcanism Program provides compiled reports of many of the Earth's volcanoes, with Nishinoshima as no exception. Contained within reports of Nishinoshima, we were able to acquire the start and end dates of the eruption, directions of lava deposition on the island, ash plume heights, and eruption style from December 2019 to October 2020. We note that GVP reports maximum and minimum plume heights within a 6-day period, such that we do not plot a specific plume height on a specific day, but a range of observed plume heights over a week. These data are present in Figure 2a. Kaneko et al. (2022) also provide an analysis of different stages of the eruption, used to determine eruption end date.

Visual observations from the Hydrographic and Oceanographic Department of the Japan Coast Guard were crucial for our early evaluations of the eruption (Japan Coast Guard, 2020, see Figures 2 and 3). We use these images to ground truth observations from the Global Volcanism Program.

We plot the Global Ocean Biogeochemistry Analysis and Forecast and Hindcast data sets to understand the background state of nutrients around Nishinoshima. These are available through the Copernicus Monitoring Environment Marine Service (E.U. Copernicus Marine Service Information (CMEMS). Marine Data Store (MDS), 2018a, 2019). This product is generated using the Pelagic Interactions Scheme for Carbon and Ecosystem Studies, available on the Nucleus for European Modeling of the Ocean (NEMO) platform and provided at a 25 km resolution. We visualize nitrate, phosphate, and other oceanographic properties to understand the background levels for these nutrients.

We used mixed layer depth and ocean currents from the Global Ocean Physics Reanalysis data set available through CMEMS (E.U. Copernicus Marine Service Information (CMEMS). Marine Data Store
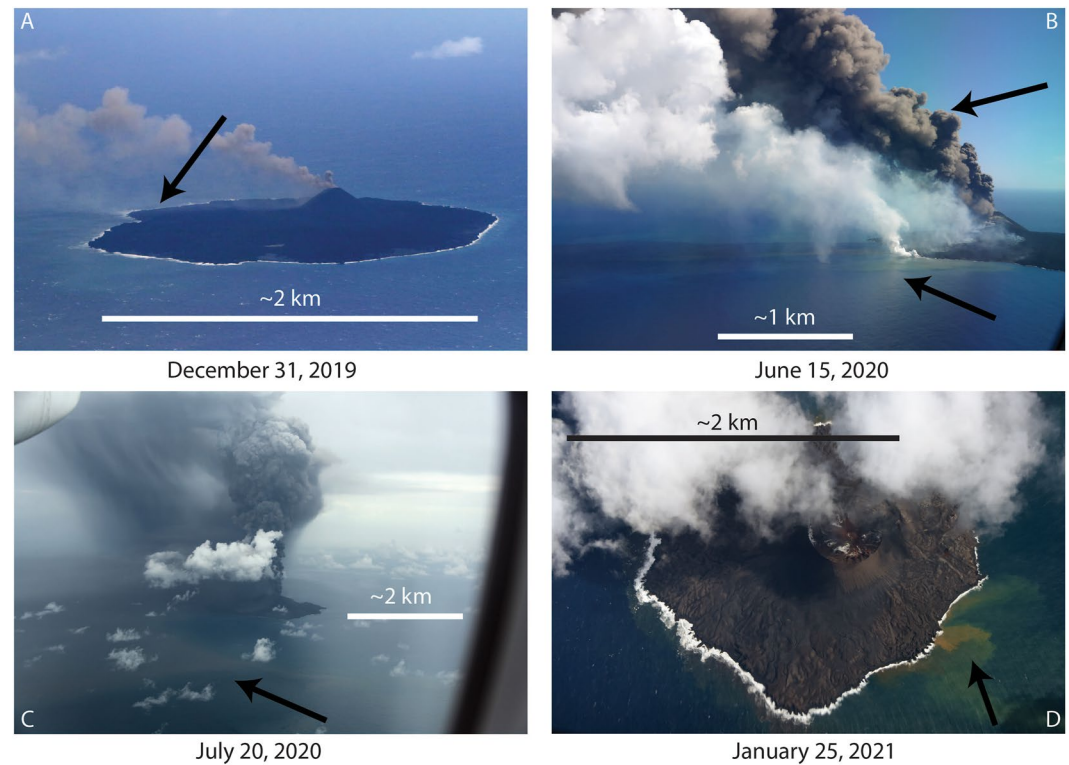
Figure 3. Aerial photos of Nishinoshima, courtesy of the Japan Coast Guard (Japan Coast Guard, 2020). a, b, and c are taken during different phases of the eruptive activity, and d is the winter after the eruptive activity, during a period of quiescence. (a) This image shows a plume rising out of the main cone, the arrow pointing to lava entry into the ocean. (b) Lava entry into the ocean with a large, dark plume present in the same direction. Discoloration in the water can be seen underneath the plumes. (c) A large dark plume is present, as well as some discoloration in the water further from the volcano. (d) Water discoloration, possibly from erosion.

(MDS), 2018b). This data set provides daily means of temperature, salinity, mixed layer depth, ocean currents, sea level, and sea ice properties at a resolution of 1/12°, or ~8 km. Mixed layer depth was visualized over the duration of the eruption as well as before and after (Figure 1b). We visualize ocean currents overtop chlorophyll-*a* concentration to understand how ocean currents relate to chlorophyll-*a* directions (Figures S5, S7, and S8 in Supporting Information S1). To account for a time delay, we overlay ocean currents from 4 days prior to the chlorophyll-*a* image. This is a reasonable assumption given that for typical ocean currents of ~0.5 m/s, a bloom will travel a few hundred km away from Nishinoshima in 4 days. This is comparable to what we see in the Chl_{Sat} data set.

3. Eruption History

The effusive phase of the 2019–2020 eruptions of Nishinoshima, which is defined as the Episode 4 eruption of Nishinoshima (Kaneko et al., 2022; Maeno et al., 2021), began on 4 December 2019 (Figure 2a). Continuous lava flows began on 5 December (Kaneko et al., 2022). A summary of the eruptive history is available in Figure 2. Deposition of lava in this earliest phase was on the western and eastern sides of the island. Deposition directions of lava were determined by examining biweekly SAR images from JAXA's ALOS (DAICHI)-2 satellite (Geospatial Information Authority of Japan, 2020), with primary deposition directions to the north. Over the next 5 months, activity was primarily effusive, with 4 instances of ash plumes 1–3 km in height erupting over short-lived periods (Figure 2a; Global Volcanism Program, 2020). Strombolian activity occurred frequently during the period as well (Kaneko et al., 2022). Beginning in June 2020, ash plumes co-occurred more frequently with lava deposition into the ocean. Continuous ash venting, observed in aerial and satellite imagery, began in earnest mid-June 2020, with plume heights mostly from 2 to 6 km. A single plume rose to 8 km in height on 3 July 2020. During this time, from late June to mid-July 2020, lava fountain activity occurred that increased the size of the pyroclastic cone,

along with the emission of dark ash clouds (Kaneko et al., 2022; Maeno et al., 2021). This period also coincided with the maximum effusion rates for the whole eruption, before a sharp drop-off (Kaneko et al., 2022). Plume heights and dates, as well as their associated uncertainties are present in Figure 2a.

New lava deposition ceased in the beginning of July 2020, with the eruption shifting fully to explosive behavior that Kaneko et al. (2022) suggested is phreatomagmatic due to the release of fine ash and decrease in effusion rate. From aerial images, ash fallout deposits can be seen on the surface of the island starting in June 2020 (Maeno et al., 2021). We also interpreted areas of low reflection intensity in SAR images as areas of ash deposition. By mid-August 2020, ash plumes ceased. Over the next few months, gas plumes continued to be emitted from the vent on Nishinoshima, with eruptive activity largely ceasing on August 20th 2020 and fumarolic activity continuing to be present inside the crater, seen through aerial observation by the Japan Coast Guard (Global Volcanism Program, 2020; Japan Coast Guard, 2020; Kaneko et al., 2022).

4. Chl_{Sat} Response to Eruption

We observe a positive response to the explosive phase of the 2019–2020 eruption in all four products we use to assess phytoplankton. Specifically, $Chl_{SatMODIS}$ and POC_{Sat} concentrations from MODIS (Figure 4c) and Chl_{Sat} and F_{Sat} from OLCI (Figure 5) increase during the explosive phase of the 2019–2020 eruption. Averaged $Chl_{SatMODIS}$ during the effusive phase of the eruption is 0.1 mg/m^3. During the explosive phase, the average $Chl_{SatMODIS}$ increases to 0.6 mg/m^3. From mid-August to December 2020, after the explosive phase of the eruption, the average is 0.08 mg/m^3. The average 95th percentile of Chl_{Sat} during the explosive phase of the eruption is 1.23 mg/m^3. During the same period in the summer of 2021, the average is only 0.08 mg/m^3. In the months before the explosive eruption, Chl_{Sat} had an average 95th percentile of 0.15 mg/m^3. After the explosive eruption ceased (mid-August–end of October 2020), the average 95th percentile of Chl_{Sat} fell to 0.08 mg/m^3. To emphasize, heightened chlorophyll and fluorescence began at the same time as the explosive eruption phase in mid-June 2020 (Figures 4a and 4b) and were present throughout July and early August 2020. Figures 5c–5f shows examples of these heightened values on 9th and 25th July 2020 (Figures 5c–5f). Differences in values between $Chl_{SatMODIS}$ and Chl_{Sat} are possibly due to the difference in chlorophyll-retrieval algorithms. By inspection of our scale of Chl_{Sat} values in images from Nishinoshima (95th percentile of data >1.0 mg/m^3), we determine they are 10x the background values of ~0.1 mg/m^3 from early summer 2020 or summer 2021.

Images from mid-August 2020 show that the intensity of Chl_{Sat} values subside (Figure S2 in Supporting Information S1), as do the MODIS $Chl_{SatMODIS}$ and POC_{Sat} time series values. We conclude that the blooms lasted from mid-June to mid-August 2020. This is different from previous studies, which focused on single-event eruptions and blooms that lasted for a couple of weeks at most (Barone et al., 2022; Lin et al., 2011; Olgun et al., 2013). Compared to the size of phytoplankton blooms observed following the 2018 eruption of Kilauea, maximum chlorophyll extents of Nishinoshima were ~250 km long, larger than the 150 km lateral extent from the Kilauea event (Wilson et al., 2019). Observed Chl_{Sat} concentrations in the Nishinoshima blooms are also an order of magnitude higher than those determined from MODIS from 2018 Kilauea chlorophyll images (maximums >0.2 mg/m^3). These differences in concentration may be partly due to the use of different algorithms (MODIS vs. POLYMER). Still, the Nishinoshima bloom was much larger at its maximum (250 vs. 150 km) than the Kilauea bloom.

4.1. Establishment (and Onset) of Chlorophyll as Biologic

To confirm whether increases in Chl_{Sat} seen at Nishinoshima are biological in nature, F_{Sat} is calculated using the OC-Fluo algorithm (Kritten et al., 2020). The F_{Sat} imagery shows that these increases in chlorophyll are indeed biological because of a concurrent increase in fluorescence values by at least a factor of 4 (0.2 vs. 0.8–1.4 mW nm^{-1} m^{-1} sr^{-1}). Specifically, before the presence of chlorophyll signatures in the water (as determined by POLYMER Chl_{Sat} images), F_{Sat} values are unelevated (Figures 5a and 5b). Only when the satellite imagery shows elevated Chl_{Sat} do F_{Sat} values also increase (Figures 5c–5f; Figure S3 in Supporting Information S1). Heightened fluorescence relative to background is known to result from phytoplankton blooms because fluorescence is the light re-emitted from chlorophyll-a that is not used for photosynthesis (Letelier & Abbott, 1996). Thus, the elevated Chl_{Sat} values we observe are from phytoplankton, not just due to water discoloration from ash. Spectra of the bloom area are also in line with spectra of heightened chlorophyll-a (see Figure S4 in Supporting Information S1; Whiteside et al., 2023).
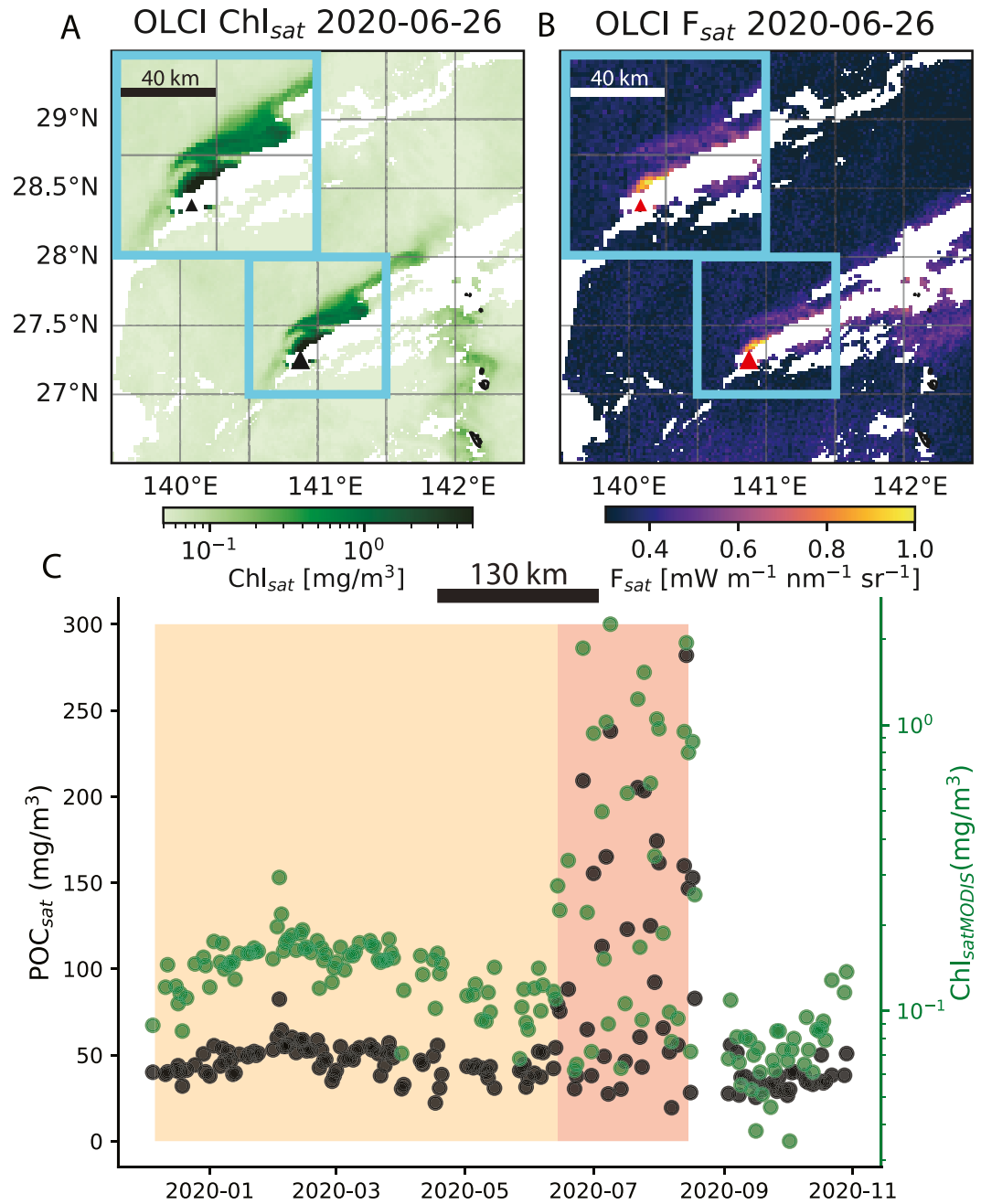
Figure 4. Chlorophyll-*a* (a) and Fluorescence (b) imagery from 26 June 2020. Chl_{Sat} increases are represented in dark green, F_{Sat} increases are represented in lighter purples, oranges, and yellows. Increases in Chl_{Sat} correspond with increases in F_{Sat} based on the imagery. It can be seen that the increases in $Chl_{SatMODIS}$ and POC_{Sat} (c) occur when increases in chlorophyll concentration and fluorescence appear in full. Increases in fluorescence in (b) are seen by the bright yellow/orange and light purple region in the inset. The yellow box shows the effusive-only activity at Nishinoshima. The red box shows the time of explosive activity at Nishinoshima. The images in (a) and (b) occur within the red box in (c).

4.2. Spatial Relationship of Phytoplankton With Ash

The areas of heightened Chl_{Sat} and F_{Sat} correlate with ash plume direction (Figures 6 and 7). Ash plumes (pink/magenta) in late June 2020 are directed toward the Northeast relative to Nishinoshima, which is where the highest chlorophyll values are present (Figures 6a and 6b). Ash plumes then shift to the Northwest and high chlorophyll values appear in that direction starting around 5th July 2020. Subsequently, high chlorophyll values Northeast of the island dissipate (Figures 6c and 6d). By 17th July 2020, ash plumes move to the North-Northeast once again
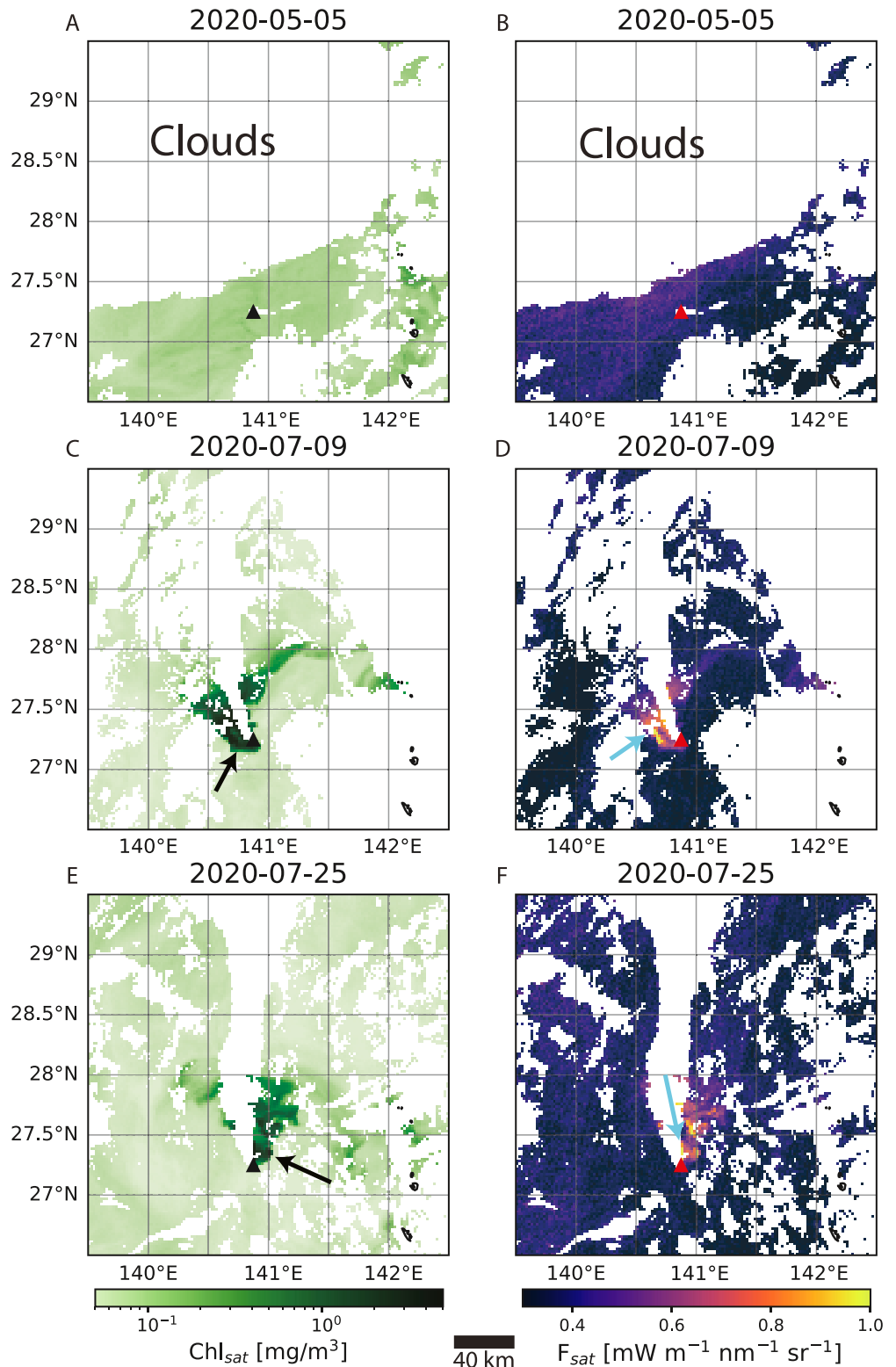
Figure 5. Chlorophyll (a, c, e) and Fluorescence (b, d, f) imagery from 3 days during the spring/summer of 2020. Before the explosive phase of the eruption, chlorophyll and fluorescence increases are not seen in any pattern (a, b). Upon the onset of the explosive phase, the chlorophyll and fluorescence increases are present and similar in morphology (c, d). By 25th July, this relationship between chlorophyll concentration and fluorescence is clearer, with fluorescence very distinct from the background (e, f). Arrows guide the eyes to the feature described.
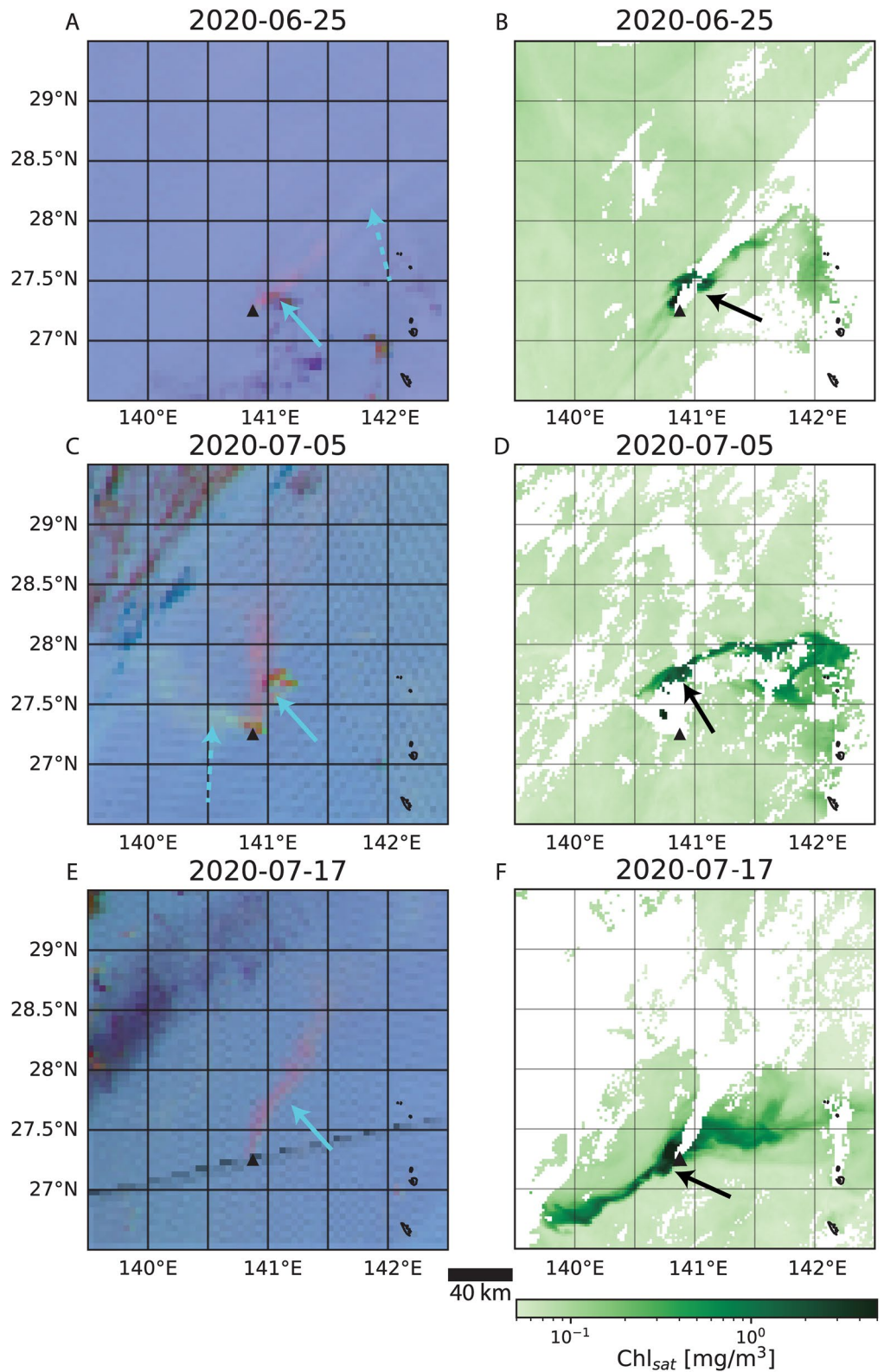
Figure 6. Ash/SO$_2$ red-green-blue (RGB) imagery developed using MODIS (a, c, e) and corresponding chlorophyll imagery (b, d, f). In Ash/SO$_2$ RGB images, pink areas show ash, green areas show SO$_2$, and yellow areas show a mix between ash and SO$_2$. Dashed lines in images (a, c, e) indicate green/yellow areas, and solid lines indicate pink areas.

Figure 7. Ash Plume directions (red, bottom) and maximum chlorophyll-*a* directions (green, top) determined from Ash/SO₂ red-green-blue (RGB) and chlorophyll POLYMER images, respectively. Arrows show the estimated direction of ash/chlorophyll, filled circles show days without ash plumes or chlorophyll-*a* increases above background present, and open circles show days when there was cloud cover over Nish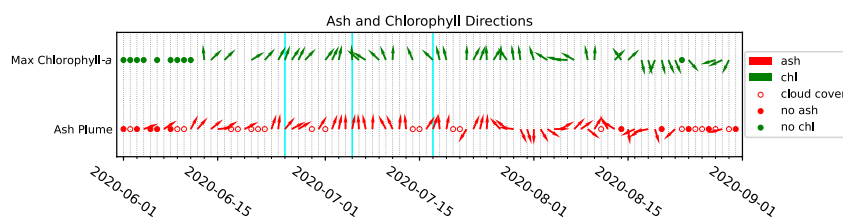inoshima, so no Ash/SO₂ RGB could be acquired. Gray vertical lines represent 1 day. Cyan lines indicate dates used in Figure 6. To view these chlorophyll images with ocean currents, view Figures S5, S7, and S8 in Supporting Information S1.

and the highest chlorophyll concentrations are also present North of Nishinoshima (Figures 6e and 6f). In general, we see that whenever the primary dispersal direction of ash plumes moves, chlorophyll follows suit within a week or less, though the exact spatial relation is modified by ash advection by surface ocean currents (Figures S5, S7, and S8 in Supporting Information S1). Although we focus on the spatial correlation, a causal link would result from ash deposition that occurs underneath the ash plumes.

We note, however, that the spatial correlation between chlorophyll and ash plume direction is imperfect. For example, Figure 6f shows chlorophyll to the SW and NE of Nishinoshima on 17 July 2020, while ash is being blown to the North-Northeast. We posit that ocean currents, affected by local storms as indicated by the high cloud cover in the 2–3 days prior to 17th July 2020, are responsible for this discrepancy. Indeed, we observe that ocean currents to the west of the island moved to the southwest in the days prior to 17th July 2020, consistent with the chlorophyll orientation in Figure 6f (Figure S5 in Supporting Information S1).

To assess ash plume and chlorophyll directionality more quantitatively, Figure 7 shows prevailing ash directions and approximate maximum chlorophyll directions relative to Nishinoshima over the explosive phase of the 2019–2020 eruption sequence. We can see that, overall, if you have ash deposition in one direction, maximum chlorophyll concentration is seen in 5 days or less afterward in a similar direction (e.g., 11th June 2020 Ash to the NE and 14th June 2020 Chl$_{Sat}$ to the NE, also see Browning et al., 2015; Lin et al., 2011; Westberry et al., 2023, 2019). We do note that there is a discrepancy in the direction of ash plumes relative to phytoplankton blooms in the beginning of August 2020 and when the explosive eruption starts to wane (Figure 7). We discuss this waning stage of the eruption below.

4.3. Relationship Between Phytoplankton and Increased SO₂ in Plume

Starting in August 2020 and during the waning phase, we start to see evidence for significant SO₂ in the ash plumes. Specifically, in the Ash/SO₂ imagery we see more green color present in the ash plumes, indicative of higher concentrations of SO₂ (Figure S6 in Supporting Information S1). The green color indicates lower ash relative to SO₂ in the plumes, although we cannot make a quantitative determination of ash and SO₂ concentrations (Gray & Bennartz, 2015). The timing of the relative increase in SO₂ in the eruption plumes in August 2020 aligns with the start of stage 3 of the eruption as defined by Kaneko et al. (2022) and the beginning of phreatomagmatic activity (Kaneko et al., 2022). We posit that the change in the eruptive style and consequently the spatial pattern of ash deposition is responsible for the lack of correlation between the direction of ash plumes relative to phytoplankton blooms in the beginning of August 2020, as well as ocean currents north of the island moving in a northward direction (Figures S6 and S7 in Supporting Information S1) (Kaneko et al., 2022).

4.4. Time Delay Between Ash Deposition and Phytoplankton Blooms

We see evidence for 3–9 days of lag between the deposition of ash and the occurrence of phytoplankton blooms. For example, it can be seen in Figure 7 that ash deposition, according to the RGB images, began on 4th June 2020. Ash plumes continued intermittently until chlorophyll concentrations increased on 13th June 2020, 9 days after imagery indicated an explosive activity. Overall, ash plumes were consistently emitted from 14th June to 13th August 2020 and that phytoplankton blooms were present between 13th June and the end of August

2020 (Figure 7; Global Volcanism Program, 2020; Kaneko et al., 2022). We also observe that areas of elevated chlorophyll-*a* concentrations correspond with ocean current directions at least 4 days prior to the day of observation (Figures S5 and S6 in Supporting Information S1). This agrees nicely with our determination of a time lag of 5 days or less (between ash deposition and bloom) based on the visual observations of the ash RGBs and the Chl$_{Sat}$ data set. This time lag estimate is also in line with typical time lags regarding ash deposition and phytoplankton blooms, with peak levels onset at a later date (Browning et al., 2015; Lin et al., 2011; Westberry et al., 2019, 2023).

4.5. Eruptions and Discolored Water at Nishinoshima in 2021

We use a brief (~1 day) explosive eruption of Nishinoshima in August 2021 to test whether ash consistently generates phytoplankton blooms. We assess the chlorophyll and fluorescence values around Nishinoshima following this eruption and find chlorophyll-*a* concentrations were elevated around Nishinoshima with a maximum of 4 mg/m^3 on 15 August 2021, with slight increases in fluorescence (Figures 8a and 8b). Before this event, chlorophyll increases are not observed. This event was very short-lived, with the eruption only occurring on 1 day, so not enough material was likely deposited to observe changes to the scale seen in the summer of 2020, both in the size of bloom as well as bloom duration.

4.5.1. Non-Eruptive Discolored Water—Biological Response?

To further test our conclusion regarding the relationship between volcanic ash and phytoplankton bloom, we analyze water discoloration around Nishinoshima that is not associated with an eruption. This allows us to test whether phytoplankton blooms can occur around Nishinoshima during volcanic quiescence. Discoloration of water was seen around Nishinoshima spanning $\emptyset(100)$ km in October 2021 and was not associated with an identifiable eruption (Figure 8c). Instead, the discolored water may be from erosion and resuspension of sediments around Nishinoshima Island by wave action or hydrothermal fluid discharge. Figure 5 images show areas of increased Chl$_{Sat}$ from the POLYMER algorithm; however, fluorescence increases were not observed above the background (0.6 mW nm^{-1} m^{-1} sr^{-1}) (Figure 8d). This lack of fluorescence indicates that the discolored water picked up by chlorophyll processing algorithms was not biologic and not a phytoplankton bloom. We further postulate that the particles in the water in October 2021, unlike the 2020 ash, did not contain the nutrients needed to trigger a phytoplankton bloom.

4.6. Summary of Results

The increases in chlorophyll concentration, POC$_{Sat}$, and fluorescence during the explosive phase of Nishinoshima's 2020 eruption indicate that there is a connection between the deposition of ash and the increase in biological activity. We can therefore answer the first two questions posed in the introduction. First, there were phytoplankton blooms that occurred during the 2019–2020 eruptive activity of Nishinoshima. Second, the phytoplankton blooms were associated with explosive eruptive activity during the summer of 2020, not effusive activity. We can address our original questions, in part, because we do not see elevated chlorophyll following lava deposition into the ocean in spring 2020 (Figures 5a and 5b). In addition, we do not see evidence that island erosion provided enough material or the right material to allow for a phytoplankton response. We now explore possible answers to our final question: (3) What are the possible mechanisms of phytoplankton bloom creation in LNLC regions?

5. Discussion

5.1. Comparison With Previous Studies

Kaneko et al. (2022) also identified the significant discoloration of ocean water during the explosive phase of Nishinoshima's 2020 eruption. They concluded, however, that the water discoloration was due to the formation of very fine, non-biologic SiO$_2$-Fe$_2$O$_3$-Al$_2$O$_3$-H$_2$O low-crystalline precipitates as a result of seawater interaction with hydrothermal fluids released coincidently with the eruption. The conclusion that the discoloration was not linked with volcanic ash drew, in part, from assessment that ash deposition direction did not line up with the orientation of the discolored water signatures (Kaneko et al., 2022, Figure 9 therein), as well as Nishinoshima residing in an LNLC region. Important to note is that any discoloration underneath the plume would not be visible, so to understand the relationship between ash and chlorophyll, one must analyze the trend over multiple
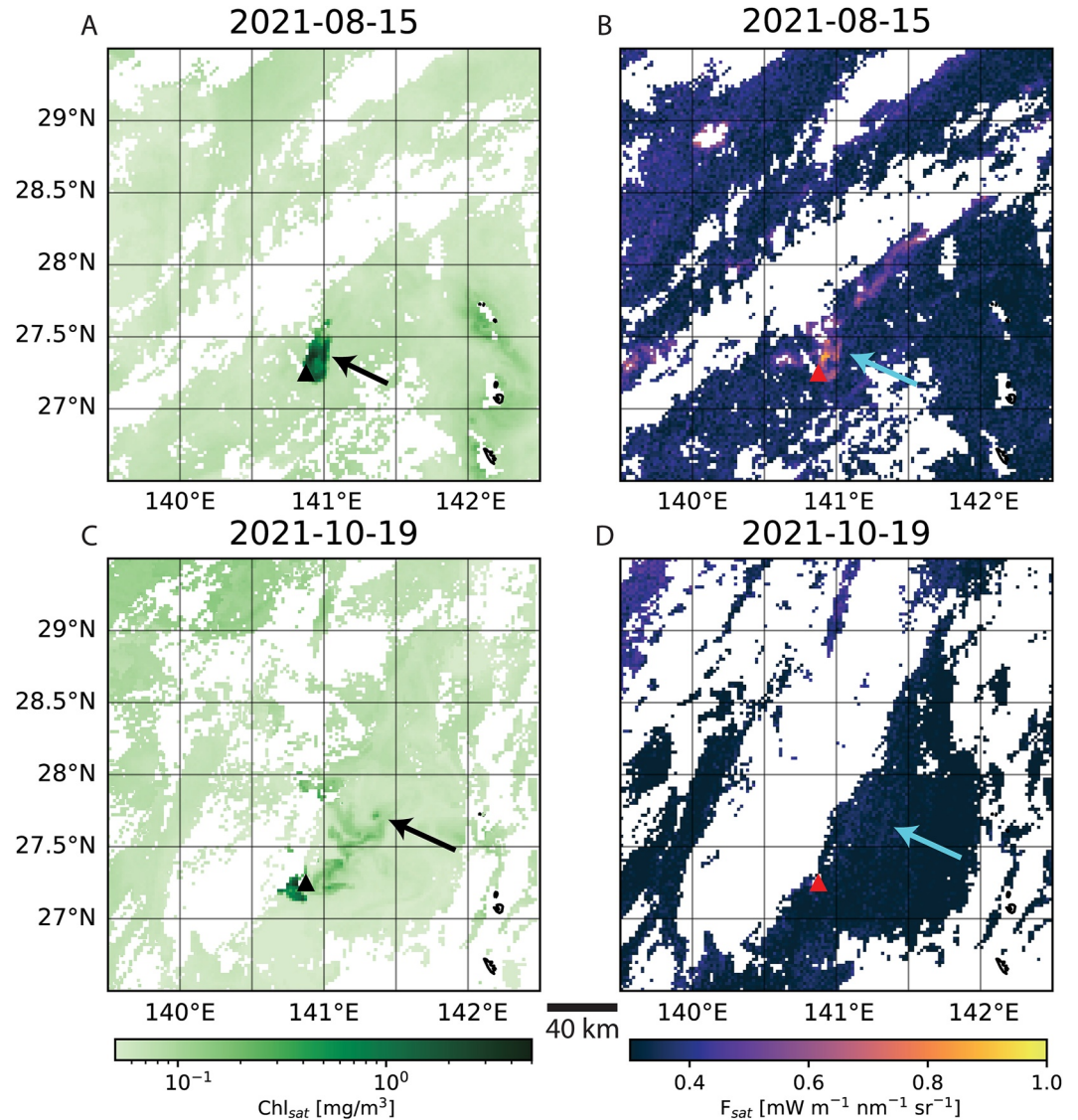
Figure 8. Chlorophyll (a, c) and Fluorescence (b, d) images from 15 August 2021, and 19 October 2021. Shortly after the eruption of Nishinoshima in 2021, which was short-lived, elevated chlorophyll and fluorescence were seen in the ocean around the Island. These largely dissipated after a few days. There was discoloration in the water due to hydrothermal fluid discharge seen in mid-October 2021 (c, d). Even though increases in chlorophyll concentration are seen to 1 mg/m³, fluorescence does not increase. This lack of fluorescence implies that the chlorophyll concentration is a result of particles in the water column scattering light similarly to chlorophyll, or there has not been enough time for fluorescence to increase.

days. In contrast to the conclusions of Kaneko, Figure 7 shows that there is mostly agreement with ash's general deposition direction over time and bloom location when analyzing the full temporal sequence. We also consider the time delay between ash deposition and bloom generation and the impact of ocean currents during this lag (Figures S5, S7, and S8 in Supporting Information S1). For example, Kaneko et al. (2022) observe that on 1 July 2020, the ash plume was oriented to the north while the discoloration was oriented northeast. We note that ocean currents were moving to the northeast in late June 2020 (Figure S8 in Supporting Information S1), and that in the days before 1st July 2020 ash plumes were moving to the northeast (Figure 7), making the plume and bloom orientation largely consistent.

Independent of the bloom and plume orientation analysis, we also provide evidence that the water discoloration was biologic in nature (see Section 4.1). The positive fluorescence signatures shown here support the interpretation that the discolored water results from phytoplankton blooms rather than inorganic precipitates. Indeed,

Kaneko et al. (2022) utilized a satellite product that did not distinguish between organic and inorganic particles in the ocean and thus could not identify the discoloration as biologic. Instead, they relied on a traditional view that phytoplankton blooms are rare in oligotrophic areas (Duggen et al., 2007, 2010; Lin et al., 2011) and determined that the discolored water material was likely non-biologic. In Section 5.2 below, we detail the possible mechanisms for nutrient delivery to this oligotrophic ocean around Nishinoshima.

5.2. Process of Ash Fertilization

Our findings show that phytoplankton blooms around Nishinoshima correlate in space and time with ash deposition (with a biologically reasonable time lag). As a result, we postulate and explore further in this section the mechanism of phytoplankton bloom generation in line with the delivery of iron and other nutrients by ash, similar to the processes inferred following the Kasatochi eruption in 2008 (Langmann et al., 2010; Lindenthal et al., 2013; Westberry et al., 2019). We assume that because volcanic ash is Fe-rich, it can supply the necessary, bio-available iron (Frogner et al., 2001). However, the mechanisms through which other limited nutrients are delivered, specifically nitrogen and phosphorous, are not as well-understood (Mills et al., 2004; National Academies of Sciences, Engineering, and Medicine, 2022; Westberry et al., 2023). The goal of the following sections is to understand and estimate on an order of magnitude basis what must be possible for a phytoplankton response during the 2020 eruption of Nishinoshima, as well as highlight possible further avenues of research. In the absence of in situ measurements, we focus on calculations based off our results from satellite and model data.

Nishinoshima is located in a Low Nutrient, Low Chlorophyll (LNLC) region and subtropical gyre (Zhang et al., 2019) where all nutrients can be limiting (Zhang et al., 2019). For phytoplankton to grow, nitrogen (Sigman & Casciotti, 2001) and phosphorus (Mills et al., 2004) are critically important in addition to iron. Understanding the processes that supply phosphorus and nitrogen is thus crucial to understand the mechanism that creates phytoplankton blooms around Nishinoshima. The Anatahan study proposed that volcanic ash delivers the required phosphorus that enabled nitrogen fixation by phytoplankton to acquire needed nitrogen (Lin et al., 2011). As referenced at the end of Section 1.1, shallower mixed layers limit nutrient supply from the deeper ocean to the surface. As seen in Figure 1b, mixed layer depth around Nishinoshima in the summer of 2020 is shallow (<20 m). We also see that Chl_{Sat} follows a seasonal trend (Figure S9 in Supporting Information S1), with highest chlorophyll-a in the winter and lowest in the summer. This is opposite of what we see in 2020, where mixed layer is shallow, but chlorophyll-a is maximum. This pattern indicates the importance of surface forcing of the phytoplankton bloom due to ash deposition as phytoplankton cannot as easily access nutrients from deeper waters when mixed layer depth is shallow as it is in summer 2020 (Diaz et al., 2021; Itoh et al., 2015; Rousseaux et al., 2012; Westberry et al., 2023; see also Supporting Information S1 of Figure S10 in conjunction with Figure 1b). Since the maximum chlorophyll-a values may not be right at the surface (Chen et al., 2022), we also consider the depth of the euphotic zone when chlorophyll-a maxima are greater than 1 mg/m^3 (∼50 m or less) (Xu et al., 2022) in our calculations below.

To explore nutrient needs for phytoplankton blooms, we use the Redfield Ratio to estimate how much nitrogen and phosphorus would be needed to generate the increase in POC_{Sat} observed from satellite data at Nishinoshima. The Redfield Ratio is a well-established measure of the concentrations of carbon, nitrogen, and phosphorus in phytoplankton biomass (phytoplankton cells) (Redfield, 1934, 1958), where the ratio of C:N:P in moles is 106:16:1. The Chl:C ratio in the ocean around Nishinoshima is approximately 0.01 during the boreal summer (Arteaga et al., 2016; Furuya, 1990), which means 1 mg/m^3 of Chl corresponds to 100 mg/m^3 of C. Assuming phytoplankton in each m^3 of seawater produce on average ∼1 mg/m^3 chlorophyll, as inferred from imagery, we estimate that this chlorophyll signature corresponds to ∼100 mg/m^3 carbon or ∼8.3 mmol/m^3. Using the 8.3 mmol/m^3 carbon estimate, the Redfield ratio suggests that concentrations of N and P of ∼1.3 mmol/m^3 and ∼0.08 mmol/m^3 are needed, respectively. These N and P concentrations are 1–2 orders of magnitude higher than the background concentrations of N and P in the region around Nishinoshima, as estimated by reviewing the Global Ocean Biogeochemistry Analysis and Forecast/Hindcast data sets (E.U. Copernicus Marine Environment Monitoring Service, 2018a, 2019; see Figure S10 in Supporting Information S1 for an illustration). If instead World Ocean Atlas (WOA) is used, an observational climatology, the required concentration of N is one order of magnitude above background and the needed P is similar in concentration to that available in the form of phosphate (Boyer et al., 2018). Together, the background levels of N and P around Nishinoshima would support at most 0.3 (CMEMS) to 30 (WOA) mg/m^3 of carbon, much less than the estimated values of 100 mg/m^3 from

satellite imagery of the phytoplankton blooms. Thus we infer that, in the summer of 2020, external sources of N, and possibly P, were required to stimulate the observed phytoplankton blooms.

Here we explore the possibility that volcanic ash also supplied the necessary phosphorus. Previously dredged andesitic samples at Nishinoshima show the presence of P_2O_5 in erupted products in abundances of 0.07–0.32 wt % (Tamura et al., 2019), which is less than seen in some other volcanic areas (Frogner et al., 2001) but greater than P_2O_5 present in various rhyolites (see Table 1 in Tramontano et al., 2017). Although the volcanic material that erupted in 2020 was basaltic andesite (Earthquake Research Institute, 2020), if we assume that the 2020 ash had the same P_2O_5 concentrations as samples from Tamura et al. (2019), that would correspond to 1,000–5,000 μmol of Phosphorus per 100 g of ash. It has been shown that, for basaltic-andesite ash from Hekla volcano in Iceland, upon initial exposure of ash to seawater, adsorbed phosphate particles attached to ash are released at a rate of 1.7 μmol g^{-1} h^{-1} (Frogner et al., 2001). Assuming 100 g of ash was continuously deposited over 10 cubic meters of water (e.g., 1 m^2 area i.e., 10 m deep, the approximate mixed layer depth in the region (Figure 1b) (de Boyer Montégut et al., 2004, 2022), it would take about 4.1 hr for phosphorus concentrations to reach values estimated using the Redfield Ratio. Using a maximum of 100 m, accommodating deeper euphotic zones (Chen et al., 2022; Dai et al., 2023 and references therein; Xu et al., 2022), this becomes 41 hr, or almost 2 days. Thus, it is possible that the required phosphorus was supplied by volcanic ash, which was deposited by ash plumes from mid-June to mid-August 2020.

Another possible source of phosphorus is Dissolved Organic Phosphorus (DOP). DOP differs from the phosphorus that is estimated by the Global Ocean Biogeochemistry Analysis and Forecast/Hindcast data sets in that the values in the latter are modeled values of phosphate in the ocean, which is a different form of phosphorus than DOP. DOP is a major support for primary production in oligotrophic areas of the ocean (Björkman & Karl, 2003; Lomas et al., 2010; Mather et al., 2008). In areas where iron is not under stress but phosphate is under stress, DOP is consumed for primary production (Liang et al., 2022). There is evidence that DOP concentrations near Nishinoshima can be as much as 0.15 μM (mmol/m^3) (Liang et al., 2022), which is more than the required P concentration estimated above of 0.08 mmol/m^3. Thus, it is possible that the phytoplankton blooms utilized DOP.

Volcanic ash may not, however, be able to provide the necessary nitrogen. The nitrogen output of the entire Izu-Bonin-Mariana Arc is thought to be 1.3×10^8 mol/yr (Li & Li, 2022), but Nishinoshima products have not been analyzed for nitrogen. As a result, we suggest that the phytoplankton identified in this study may be nitrogen-fixing. Biological N_2-fixation is the process where dinitrogen gas is converted into a form that is usable by plants (Bohlool et al., 1992). Some types of phytoplankton, such as *Trichodesmium* spp., acquire nitrogen through nitrogen fixation (Mague et al., 1977). Nitrogen-fixing phytoplankton are not rare; up to half of the yearly N fluxes are due to N_2-fixation in oligotrophic areas (Karl et al., 1997). Duggen et al. (2007) showed through experiments that the deposition of ash mobilizes fixed nitrogen. Lin et al. (2011) conclude, for example, that the spectral signature of the 2003 Anatahan bloom was consistent with that of *Trichodesmium* and that volcanic ash increased nitrogen fixation. N_2-fixation by phytoplankton could therefore facilitate the chlorophyll increases observed during the explosive phase of the 2019–2020 eruption of Nishinoshima (Duggen et al., 2007; Lin et al., 2011). Future blooms at Nishinoshima could be sampled to test this idea and determine the specific species responsible for blooms around Nishinoshima.

5.3. Implications

Phytoplankton blooms can have impacts on carbon sequestration. Phytoplankton are a key factor in the biological carbon pump, which controls how CO_2 is transferred from the atmosphere to the oceans and seafloor sediments (Ducklow et al., 2001; Volk & Hoffert, 1985). Although volcanic eruptions are common, with more than a dozen occurring on an average day (Global Volcanism Program, 2022), volcanic ash receives considerably less attention than dust as a mechanism for phytoplankton fertilization.

Here we estimate the output, drawdown, and net flux of carbon by the 2020 Nishinoshima eruption and corresponding phytoplankton blooms. First, we use measurements of SO_2 from the eruption to estimate total carbon output because CO_2 can be estimated from SO_2 concentrations in volcanic gases (Aiuppa et al., 2019). The emission rate of SO_2 during the explosive phase of the 2019–2020 eruption was estimated to be 10 kt/day emission of SO_2 for 60 days (Kaneko et al., 2022). Using the CO_2/SO_2 ratio for the arc where Nishinoshima is located (~2–4, Aiuppa et al. (2019)), we utilize the ratio of 2:1 and calculate (roughly) 1.2×10^{12} g of CO_2, and thus 3.1×10^{11} g of C, was emitted during the explosive phase of the eruption of Nishinoshima.

To estimate carbon drawdown by the phytoplankton blooms, we multiply the observed concentration of phytoplankton carbon by the volume of the bloom

$$\Delta C = \tau R H A D k t \tag{1}$$

where ΔC is the total amount of carbon sequestered by the bloom (grams), τ is the timescale of conversion of inorganic to organic carbon, estimated as unity (day^{-1}), R is the Chlorophyll-a to Phytoplankton Carbon ratio (unitless), H is a representative value for the satellite-derived chlorophyll concentration (mg/m^3), A is the surface area of the bloom (m^2), D is the mixed layer depth (m), k is the fraction of sinking carbon preserved in deep sediment (unitless), and t is the total duration of the bloom (days). There is uncertainty in many of the variables in Equation 1. For example, we consider a minimum mixed layer depth of 10 m (Figure 1b) and a maximum of 100 m, accommodating deeper euphotic zones and possible chlorophyll maxima in deeper waters (Chen et al., 2022; Dai et al., 2023 and references therein; Xu et al., 2022). The Chlorophyll-a to Phytoplankton Carbon ratio is 1:100 in waters close to Nishinoshima (Arteaga et al., 2016; Furuya, 1990). We utilize a daily value of 0.8 mg/m^3 by taking the average of chlorophyll-a close to Nishinoshima (within 50 km where the majority of the blooms are located) and estimate a daily bloom area of order 5,000 km^2 from visual imagery.

Not all carbon generated at the surface ocean reaches the ocean floor due to the oxidation of C into the water column leading to C dissolution (Wood et al., 2023). This dissolution of C back into the water column leads to a maximum of 20% of C preserved in sediments from the surface in the deep ocean and up to 80% in the shallow ocean. It is possible to have greater preservation, since some studies have suggested that iron and volcanic ash can significantly enhance carbon storage (Li et al., 2023). The turnover timescale is also something that is not well constrained and an accurate estimate requires a detailed understanding of the ecosystem (Filstrup et al., 2014; Yacobi & Zohary, 2010). For our order of magnitude estimate, we assume complete turnover daily, that is, the whole bloom replenishes each day based on growth and loss of phytoplankton equal to unity (Behrenfeld & Boss, 2018).

Using the estimates above, we calculate a total carbon drawdown of 4.8×10^{10}–1.9×10^{12} g. This carbon drawdown calculation shows that the phytoplankton bloom can possibly mediate carbon released from the eruption (see above). Our estimate of total carbon drawdown is 2–4 orders of magnitude smaller than the global yearly delivery of carbon from the mixed layer to the deeper ocean as a result of the ocean biological pump (5×10^{14} g, Dall'Olmo et al., 2016). When comparing to the eruption of Kasatochi and its associated C export of $\sim 1 \times 10^{13}$ g, the C export from Nishinoshima is still an order of magnitude smaller even at the upper limit (Hamme et al., 2010). Additionally, our calculated values are only 0.002%–0.1% of total 2 Pg C of anthropogenic CO_2 taken in yearly by the ocean (Manning & Keeling, 2006), However, the total C sequestration by the Nishinoshima bloom is still a large C mass. It is larger than the total sequestered C by the largest operational geological C storage project Carbfix in Iceland, which has sequestered $\sim 2.5 \times 10^{10}$ g of C over its entire operation (2014 to end of July 2023) (Carbfix hf., 2023). Additionally, the phytoplankton bloom likely mediated the net atmospheric carbon output of the Nishinoshima eruption since the bloom C export was comparable (or even much larger) than the estimated C emissions from the eruptions.

The 2018 Kilauea eruption is another eruption where phytoplankton blooms have been suggested to mediate the carbon outputs of the eruption (Wilson et al., 2019). Not only was the 2020 Nishinoshima phytoplankton bloom larger than the 2018 Kilauea bloom, but ash deposition should have had a greater impact than ocean upwelling on carbon sequestration. For the 2018 Kilauea eruption, the upwelling of nutrient-rich water, which triggered the bloom, would deliver not only limited nutrients but also carbon to the ocean surface. In contrast, ash delivery and stimulation of N_2-fixers causes no movement of carbon from below, so the phytoplankton blooms due to ash fertilization could be more likely to create a net sink of carbon. This process of stimulation of N_2-fixers is a possible important process in LNLC regions (Westberry et al., 2023), and the ecological importance of the addition of N into the ocean can be investigated to understand its impacts on overall nutrient usage (Tagliabue et al., 2023; Wyatt et al., 2023).

5.4. Future Directions

Our study utilizes the ability of satellite remote sensing to determine that the deposition of volcanic ash triggered phytoplankton blooms in the water surrounding Nishinoshima over the summer of 2020. Our study, and other

studies like it, would be enhanced by in situ measurements of nutrients, chlorophyll, and ash concentrations in the ocean. In future studies, water sampling would allow for the assessment of phytoplankton species, helping to further disentangle the relationship between discolored water and chlorophyll concentration. Although future eruptions at Nishinoshima are uncertain, its proclivity toward eruption since 2013 (Kaneko et al., 2019; Shinohara et al., 2017) makes it a good candidate for understanding the impact volcanoes can have on ocean biogeochemistry in LNLC areas using both remote sensing and in situ measurements.

6. Conclusion

The explosive and effusive phases of the 2019–2020 eruptive period at Nishinoshima Volcano, Japan, provide unique natural laboratories to examine the impacts of the volcanic activity on phytoplankton in LNLC regions. We find, using satellite products from MODIS and Sentinel-3 OLCI, that the deposition of volcanic ash correlates in space and time with increases in Chl_{Sat}. In contrast, the deposition of lava does not correlate with increases in Chl_{Sat}. To distinguish water discolored by inorganic particulates from phytoplankton blooms, we complement our Chl_{Sat} with a fluorescence product generated using the OC-Fluo algorithm (Figures 4 and 5). Because biological material fluoresces while inorganic material does not, our F_{Sat} calculation allows us to establish that the areas of elevated chlorophyll are, at least partially, phytoplankton blooms, and not entirely due to discoloration by ash. Together, our investigation demonstrates that ash deposition drives the biological response at Nishinoshima in June–August 2020.

We further explore the processes that would allow ocean nutrient concentrations to be sufficient to trigger phytoplankton blooms. We conclude that it is possible for volcanic ash to supply the needed iron and phosphorus to the surface ocean, but that the water around Nishinoshima would remain nitrogen limited due to its location in an LNLC region. Thus, we suggest that the observed blooms may have been of nitrogen-fixing phytoplankton and may have led to carbon drawdown on the order of 10^{10-12} g, possibly balancing carbon output from the eruption.

This study provides a months-long account of increases in biological activity in an LNLC region because of volcanic ash deposition. Overall, we show that the volcanically triggered phytoplankton blooms around Nishinoshima volcano resulted in significant carbon drawdown. Our findings highlight the important connections between volcanism and Earth's climate system. We emphasize that the possibility of volcanically triggered phytoplankton blooms cannot be neglected in LNLC regions, which make up large proportions of oceans on Earth. Overall, we call for long-term monitoring of ocean biogeochemistry around Nishinoshima to gain a more complete understanding of the ocean state before, during, and after an eruption.

Data Availability Statement

Satellite data used to generate POLYMER chlorophyll-*a* and Fluorescence images were acquired from the European Space Agency Ocean Virtual Laboratory and EUMETSAT Data Centre (ESA & EUMETSAT, 2022). Chlorophyll-*a* and Fluorescence products were generated according to the methodology in this manuscript, as well as Steinmetz et al. (2011) for POLYMER and Kritten et al. (2020) for fluorescence. MODIS Aqua satellite data were acquired from NASA (MODIS Characterization Support Team (MCST), 2017), and was used to generate Ash/SO_2 RGBs following the procedure outlined in the methods of this manuscript and Gray and Bennartz (2015). The 2018 reprocessing version of MODIS Aqua chlorophyll-*a* (NASA Goddard Space Flight Center, Ocean Ecology Laboratory, 2022a) and particulate organic carbon (NASA Goddard Space Flight Center, Ocean Ecology Laboratory, 2022b) products were acquired using Google Earth Engine (Gorelick et al., 2017). The Algorithm Theoretical Basis Documents (ATBDs) for the 2018 reprocessing are no longer available, but Earth Engine still uses the 2018 reprocessing at the time of publication. The current ATBDs from the 2022 reprocessing have been cited and comparisons between the 2022 and 2018 reprocessings are provided by NASA (NASA Goddard Space Flight Center, Ocean Biology Processing Group, 2022c). Effusion rates are available in Kaneko et al. (2022), and plume heights are available in the Global Volcanism program reports on Nishinoshima (Global Volcanism Program, 2020). Aerial photographs courtesy of the Japan Coast Guard (Japan Coast Guard, 2020). SAR images are available courtesy of the Geospatial Information Authority of Japan (Geospatial Information Authority of Japan, 2020). Copernicus Marine Environment Monitoring Service provides global ocean biogeochemistry and ocean physics data sets used in this manuscript (E.U. Copernicus Marine Service Information (CMEMS). Marine Data Store (MDS), 2018a, 2018b, 2019). World Ocean Atlas provides

observational climatology (Boyer et al., 2018). Figures were created using python with matplotlib version 3.6.2 (Caswell et al., 2022) and cartopy version 0.21.0 (Elson et al., 2022). Accompanying datasets and code are available on Zenodo (https://doi.org/10.5281/zenodo.8400848).

References

Aiuppa, A., Fischer, T. P., Plank, T., & Bani, P. (2019). CO_2 flux emissions from the Earth's most actively degassing volcanoes, 2005–2015. *Scientific Reports*, *9*, 5442. https://doi.org/10.1038/s41598-019-41901-y

Arteaga, L., Pahlow, M., & Oschlies, A. (2016). Modeled Chl:C ratio and derived estimates of phytoplankton carbon biomass and its contribution to total particulate organic carbon in the global surface ocean. *Global Biogeochemical Cycles*, *30*(12), 1791–1810. https://doi.org/10.1002/2016GB005458

Barone, B., Letelier, R. M., Rubin, K. H., & Karl, D. M. (2022). Satellite detection of a massive phytoplankton bloom following the 2022 submarine eruption of the Hunga Tonga-Hunga Ha'apai Volcano. *Geophysical Research Letters*, *49*(17), e2022GL099293. https://doi.org/10.1029/2022GL099293

Basu, S., & Mackey, K. R. M. (2018). Phytoplankton as key mediators of the biological carbon pump: Their responses to a changing climate. *Sustainable Times*, *10*(3), 869. https://doi.org/10.3390/su10030869

Behrenfeld, M. J., & Boss, E. S. (2018). Student's tutorial on bloom hypotheses in the context of phytoplankton annual cycles. *Global Change Biology*, *24*(1), 55–77. https://doi.org/10.1111/gcb.13858

Björkman, K. M., & Karl, D. M. (2003). Bioavailability of dissolved organic phosphorus in the euphotic zone at Station ALOHA, North Pacific Subtropical Gyre. *Limnology & Oceanography*, *48*(3), 1049–1057. https://doi.org/10.4319/lo.2003.48.3.1049

Black, B., Mittal, T., Lingo, F., Walowski, K., & Hernandez, A. (2021). Assessing the environmental consequences of the generation and alteration of mafic volcaniclastic deposits during large igneous province emplacement. *Large Igneous Provinces: A Driver of Global Environmental and Biotic Changes*, 117–131. https://doi.org/10.1002/9781119507444.ch5

Blain, S., Quéguiner, B., Armand, L., Belviso, S., Bombled, B., Bopp, L., et al. (2007). Effect of natural iron fertilization on carbon sequestration in the Southern Ocean. *Nature*, *446*(7139), 1070–1074. https://doi.org/10.1038/nature05700

Bohlool, B. B., Ladha, J. K., Garrity, D. P., & George, T. (1992). Biological nitrogen fixation for sustainable agriculture: A perspective. *Plant and Soil*, *141*(1–2), 1–11. https://doi.org/10.1007/BF00011307

Boyer, T. P., Garcia, H. E., Locarnini, R. A., Zweng, M. M., Mishonov, A. V., Reagan, J. R., et al. (2018). World Ocean Atlas 2018. Nitrate, phosphate [Dataset]. NOAA National Centers for Environmental Information. Retrieved from https://www.ncei.noaa.gov/archive/accession/NCEI-WOA18

Browning, T. J., Stone, K., Bouman, H. A., Mather, T. A., Pyle, D. M., Moore, C. M., & Martinez-Vicente, V. (2015). Volcanic ash supply to the surface ocean-remote sensing of biological responses and their wider biogeochemical significance. *Frontiers in Marine Science*, *2*, 14. https://doi.org/10.3389/fmars.2015.00014

Carbfix hf. (2023). Carbfix. [WWW Document]. Retrieved from https://www.carbfix.com

Caswell, T. A., Lee, A., Droettboom, M., de Andrade, E. S., Hoffmann, T., Klymak, J., et al. (2022). matplotlib/matplotlib: REL: v3.6.2 (v3.6.2) [Software]. Zenodo. https://doi.org/10.5281/zenodo.7275322

Chen, J., Gong, X., Guo, X., Xing, X., Lu, K., Gao, H., & Gong, X. (2022). Improved perceptron of subsurface chlorophyll maxima by a deep neural network: A case study with BGC-Argo float data in the northwestern Pacific Ocean. *Remote Sensing*, *14*(3), 59–73. https://doi.org/10.3390/rs14030632

Dai, M., Luo, Y., Achterberg, E. P., Browning, T. J., Cai, Y., Cao, Z., et al. (2023). Upper ocean biogeochemistry of the oligotrophic North Pacific Subtropical Gyre: From nutrient sources to carbon export. *Reviews of Geophysics*, *61*(3), e2022RG000800. https://doi.org/10.1029/2022RG000800

Dall'Olmo, G., Dingle, J., Polimene, L., Brewin, R. J. W., & Claustre, H. (2016). Substantial energy input to the mesopelagic ecosystem from the seasonal mixed-layer pump. *Nature Geoscience*, *9*(11), 820–823. https://doi.org/10.1038/ngeo2818

de Boyer Montégut, C. (2022). Mixed layer depth climatology computed with a density threshold criterion of 0.03kg/m³ from 10 m depth value. *SEANOE*. https://doi.org/10.17882/91774

de Boyer Montégut, C., Madec, G., Fischer, A. S., Lazar, A., & Iudicone, D. (2004). Mixed layer depth over the global ocean: An examination of profile data and a profile-based climatology. *Journal of Geophysical Research*, *109*, C12003. https://doi.org/10.1029/2004JC002378

Diaz, B. P., Knowles, B., Johns, C. T., Laber, C. P., Bondoc, K. G. V., Haramaty, L., et al. (2021). Seasonal mixed layer depth shapes phytoplankton physiology, viral production, and accumulation in the North Atlantic. *Nature Communications*, *12*(1), 6634. https://doi.org/10.1038/s41467-021-26836-1

Ducklow, H. W., Steinberg, D. K., & Buesseler, K. O. (2001). Upper ocean carbon export and the biological pump. *Oceanography*, *14*(4), 50–58. https://doi.org/10.5670/oceanog.2001.06

Duggen, S., Croot, P., Schacht, U., & Hoffmann, L. (2007). Subduction zone volcanic ash can fertilize the surface ocean and stimulate phytoplankton growth: Evidence from biogeochemical experiments and satellite data. *Geophysical Research Letters*, *34*, L01612. https://doi.org/10.1029/2006GL027522

Duggen, S., Olgun, N., Croot, P., Hoffmann, L., Dietze, H., Delmelle, P., & Teschner, C. (2010). The role of airborne volcanic ash for the surface ocean biogeochemical iron-cycle: A review. *Biogeosciences*, *7*(3), 827–844. https://doi.org/10.5194/bg-7-827-2010

Earthquake Research Institute. (2020). [Research bulletin] Nishinoshima 2019-2020 activity observation. [WWW Document]. Retrieved from https://www.eri.u-tokyo.ac.jp/news/11621/

Elson, P., de Andrade, E. S., Lucas, G., May, R., Hattersley, R., Campbell, E., et al. (2022). SciTools/cartopy: v0.21.0 (v0.21.0) [Software]. Zenodo. https://doi.org/10.5281/zenodo.7065949

ESA and EUMETSAT. (2022). S3 product notice—OLCI. [WWW Document]. Retrieved from https://sentinel.esa.int/documents/247904/4755279/S3.PN.OLCI-L1.09+-+i1r0+-+OLCI+L1+PB+3.02+%2820220120%29.pdf

E.U. Copernicus Marine Service Information (CMEMS). Marine Data Store (MDS). (2018a). Global Ocean Biogeochemistry Hindcast [Data set]. https://doi.org/10.48670/moi-00019

E.U. Copernicus Marine Service Information (CMEMS). Marine Data Store (MDS). (2018b). Global Ocean Physics Reanalysis [Dataset]. https://doi.org/10.48670/moi-00021

E.U. Copernicus Marine Service Information (CMEMS). Marine Data Store (MDS). (2019). Global Ocean Biogeochemistry Analysis and Forecast [Dataset]. https://doi.org/10.48670/moi-00015

EUMeTrain. (2014). SEVIRI RGB Cal module—part II, chapter V: Ash RGB. [WWW Document]. Retrieved from https://resources.eumetrain.org/data/4/410/print_5.htm

Filstrup, C. T., Hillebrand, H., Heathcote, A. J., Harpole, W. S., & Downing, J. A. (2014). Cyanobacteria dominance influences resource use efficiency and community turnover in phytoplankton and zooplankton communities. *Ecology Letters*, *17*(4), 464–474. https://doi.org/10.1111/ele.12246

Frogner, P., Gíslason, S. R., & Óskarsson, N. (2001). Fertilizing potential of volcanic ash in ocean surface water. *Geology*, *29*(6), 487–490. https://doi.org/10.1130/0091-7613(2001)029<0487:FPOVAI>2.0.CO;2

Furuya, K. (1990). Subsurface chlorophyll maximum in the tropical and subtropical western Pacific Ocean: Vertical profiles of phytoplankton biomass and its relationship with chlorophyll a and particulate organic carbon. *Marine Biology*, *107*(3), 529–539. https://doi.org/10.1007/BF01313438

Geospatial Information Authority of Japan. (2016). The latest survey results for Nishinoshima Island as of March 2016 are available: No major changes were identified. [WWW Document]. Retrieved from https://www.gsi.go.jp/kokusaikoryu/kokusaikoryu-e30096.html

Geospatial Information Authority of Japan. (2020). Nishinoshima DAICHI-2 SAR data analysis results (November 22, 2019-October 9, 2020). [WWW Document]. Retrieved from https://www.gsi.go.jp/BOUSAI/R1_nishinoshima.html

Global Volcanism Program. (2020). Report on Nishinoshima (Japan). In A. E. Crafford & E. Venzke (Eds.), *Bulletin of the Global Volcanism Network* (Vol. 45, Issue 9). Smithsonian Institution. https://doi.org/10.5479/si.GVP.BGVN202009-284096

Global Volcanism Program. (2022). *Current eruptions*. [WWW Document]. Smithsonian Institution. Retrieved from https://volcano.si.edu/gvp_currenteruptions.cfm#:~:text=Detailed%20statistics%20are%20not%20kept,is%20available%20for%20recent%20years

Gorelick, N., Hancher, M., Dixon, M., Ilyushchenko, S., Thau, D., & Moore, R. (2017). Google Earth engine: Planetary-scale geospatial analysis for everyone. *Remote Sensing of Environment*, *202*, 18–27. https://doi.org/10.1016/j.rse.2017.06.031

Gray, T. M., & Bennartz, R. (2015). Automatic volcanic ash detection from MODIS observations using a back-propagation neural network. *Atmospheric Measurement Techniques*, *8*(12), 5089–5097. https://doi.org/10.5194/amt-8-5089-2015

Gupta, A. K., Bennartz, R., Fauria, K. E., & Mittal, T. (2022). Eruption chronology of the December 2021 to January 2022 Hunga Tonga-Hunga Ha'apai eruption sequence. *Communications Earth & Environment*, *3*(1), 314. https://doi.org/10.1038/s43247-022-00606-3

Hamme, R. C., Webley, P. W., Crawford, W. R., Whitney, F. A., Degrandpre, M. D., Emerson, S. R., et al. (2010). Volcanic ash fuels anomalous plankton bloom in subarctic northeast Pacific. *Geophysical Research Letters*, *37*(19), L19604. https://doi.org/10.1029/2010GL044629

Huppert, A., Blasius, B., & Stone, L. (2002). A model of phytoplankton blooms. *The American Naturalist*, *159*(2), 156–171. https://doi.org/10.1086/324789

Itoh, S., Yasuda, I., Saito, H., Tsuda, A., & Komatsu, K. (2015). Mixed layer depth and chlorophyll a: Profiling float observations in the Kuroshio-Oyashio Extension region. *Journal of Marine Systems*, *151*, 1–14. https://doi.org/10.1016/j.jmarsys.2015.06.004

Jakobsen, H. H., & Markager, S. (2016). Carbon-to-chlorophyll ratio for phytoplankton in temperate coastal waters: Seasonal patterns and relationship to nutrients. *Limnology & Oceanography*, *61*(5), 1853–1868. https://doi.org/10.1002/lno.10338

Japan Coast Guard. (2020). Nishinoshima. [WWW Document]. Retrieved from https://www1.kaiho.mlit.go.jp/GIJUTSUKOKUSAI/kaiikiDB/kaiyo18-e1.htm

Kaneko, T., Maeno, F., Ichihara, M., Yasuda, A., Ohminato, T., Nogami, K., et al. (2022). Episode 4 (2019–2020) Nishinoshima activity: Abrupt transitions in the eruptive style observed by image datasets from multiple satellites. *Earth Planets and Space*, *74*(1), 34. https://doi.org/10.1186/s40623-022-01578-6

Kaneko, T., Maeno, F., Yasuda, A., Takeo, M., & Takasaki, K. (2019). The 2017 Nishinoshima eruption: Combined analysis using Himawari-8 and multiple high-resolution satellite images. *Earth Planets and Space*, *71*(1), 140. https://doi.org/10.1186/s40623-019-1121-8

Karl, D., Letelier, R., Tupas, L., Dore, J., Christian, J., & Hebel, D. (1997). The role of nitrogen fixation in biogeochemical cycling in the subtropical North Pacific Ocean. *Nature*, *388*(6642), 533–538. https://doi.org/10.1038/41474

Komick, N. M., Costa, M. P. F., & Gower, J. (2009). Bio-optical algorithm evaluation for MODIS for western Canada coastal waters: An exploratory approach using in situ reflectance. *Remote Sensing of Environment*, *113*(4), 794–804. https://doi.org/10.1016/j.rse.2008.12.005

Kritten, L., Preusker, R., & Fischer, J. (2020). A new retrieval of sun-induced chlorophyll fluorescence in water from ocean color measurements applied on olci l-1b and l-2. *Remote Sensing*, *12*(23), 3949. https://doi.org/10.3390/rs12233949

Langmann, B., Zakšek, K., Hort, M., & Duggen, S. (2010). Volcanic ash as fertiliser for the surface ocean. *Atmospheric Chemistry and Physics*, *10*(8), 3891–3899. https://doi.org/10.5194/acp-10-3891-2010

Lee, C. T. A., Jiang, H., Ronay, E., Minisini, D., Stiles, J., & Neal, M. (2018). Volcanic ash as a driver of enhanced organic carbon burial in the Cretaceous. *Scientific Reports*, *8*, 4197. https://doi.org/10.1038/s41598-018-22576-3

Letelier, R. M., & Abbott, M. R. (1996). An analysis of chlorophyll fluorescence algorithms for the moderate resolution imaging spectrometer (MODIS). *Remote Sensing of Environment*, *58*(2), 215–223. https://doi.org/10.1016/S0034-4257(96)00073-9

Li, K., & Li, L. (2022). Nitrogen enrichments in sheeted dikes and gabbros from DSDP/ODP/IODP Hole 504B and 1256D: Insights into nitrogen recycling in Central America and global subduction zones. *Geochimica et Cosmochimica Acta*, *335*, 197–210. https://doi.org/10.1016/j.gca.2022.08.036

Li, L., He, W., Liu, Z., Song, Y., Li, Y., Belousova, E., et al. (2023). Volcanic activity drives lacustrine carbon sequestration after Oceanic Anoxic Event 1a. *Palaeogeography, Palaeoclimatology, Palaeoecology*, *621*, 111595. https://doi.org/10.1016/j.palaeo.2023.111595

Liang, Z., Letscher, R. T., & Knapp, A. N. (2022). Dissolved organic phosphorus concentrations in the surface ocean controlled by both phosphate and iron stress. *Nature Geoscience*, *15*(8), 651–657. https://doi.org/10.1038/s41561-022-00988-1

Lin, I. I., Hu, C., Li, Y. H., Ho, T. Y., Fischer, T. P., Wong, G. T. F., et al. (2011). Fertilization potential of volcanic dust in the low-nutrient low-chlorophyll western North Pacific subtropical gyre: Satellite evidence and laboratory study. *Global Biogeochemical Cycles*, *25*, GB1006. https://doi.org/10.1029/2009GB003758

Lindenthal, A., Langmann, B., Pätsch, J., Lorkowski, I., & Hort, M. (2013). The ocean response to volcanic iron fertilisation after the eruption of Kasatochi volcano: A regional-scale biogeochemical ocean model study. *Biogeosciences*, *10*(6), 3715–3729. https://doi.org/10.5194/bg-10-3715-2013

Loisel, H., & Morel, A. (1998). Light scattering and chlorophyll concentration in case 1 waters: A reexamination. *Limnology & Oceanography*, *43*(5), 847–858. https://doi.org/10.4319/lo.1998.43.5.0847

Lomas, M. W., Burke, A. L., Lomas, D. A., Bell, D. W., Shen, C., Dyhrman, S. T., & Ammerman, J. W. (2010). Sargasso Sea phosphorus biogeochemistry: An important role for dissolved organic phosphorus (DOP). *Biogeosciences*, *7*(2), 695–710. https://doi.org/10.5194/bg-7-695-2010

Maeno, F., Yasuda, A., Hokanishi, N., Kaneko, T., Tamura, Y., Yoshimoto, M., et al. (2021). Intermittent growth of a newly-born volcanic island and its feeding system revealed by geological and geochemical monitoring 2013–2020, Nishinoshima, Ogasawara, Japan. *Frontiers in Earth Science*, *9*, 773819. https://doi.org/10.3389/feart.2021.773819

Maeno, F., Yasuda, A., Nakano, S., Yoshimoto, M., Ohminato, T., Watanabe, A., et al. (2018). Formation process of a new volcanic island at Nishinoshima, Ogasawara, Japan, inferred from eruptive products. *Journal of Advanced Marine Science and Technology Society*, *24*, 35–44. https://doi.org/10.14928/amstec.24.1_35

Mague, T. H., Mague, F. C., & Holm-Hansen, O. (1977). Physiology and chemical composition of nitrogen-fixing phytoplankton in the central North Pacific Ocean. *Marine Biology*, *41*(3), 213–227. https://doi.org/10.1007/BF00394908

Manning, A. C., & Keeling, R. F. (2006). Global oceanic and land biotic carbon sinks from the scripps atmospheric oxygen flask sampling network. *Tellus Series B Chemical and Physical Meteorology*, *58*(2), 95–116. https://doi.org/10.1111/j.1600-0889.2006.00175.x

Martin, J. H., & Fitzwater, S. E. (1988). Iron deficiency limits phytoplankton growth in the North-East Pacific subarctic. *Nature*, *331*(6154), 341–343. https://doi.org/10.1038/331341a0

Massonnet, D., & Feigl, K. L. (1998). Radar interferometry and its application to changes in the Earth's surface. *Reviews of Geophysics*, *36*(4), 441–500. https://doi.org/10.1029/97RG03139

Mather, R. L., Reynolds, S. E., Wolff, G. A., Williams, R. G., Torres-Valdes, S., Woodward, E. M. S., et al. (2008). Phosphorus cycling in the North and South Atlantic Ocean subtropical gyres. *Nature Geoscience*, *1*(7), 439–443. https://doi.org/10.1038/ngeo232

Mills, M. M., Ridame, C., Davey, M., La Roche, J., & Geider, R. J. (2004). Iron and phosphorus co-limit nitrogen fixation in the eastern tropical North Atlantic. *Nature*, *429*(6989), 292–294. https://doi.org/10.1038/nature02550

MODIS Characterization Support Team (MCST). (2017). MODIS 1km calibrated radiances product [Dataset]. https://doi.org/10.5067/MODIS/MYD021KM.061

Morel, A., & Prieur, L. (1977). Analysis of variations in ocean color. *Limnology & Oceanography*, *22*(4), 709–722. https://doi.org/10.4319/lo.1977.22.4.0709

Moutzouris-Sidiris, I., & Topouzelis, K. (2021). Assessment of Chlorophyll-*a* concentration from Sentinel-3 satellite images at the Mediterranean Sea using CMEMS open source in situ data. *Open Geosciences*, *13*(1), 85–97. https://doi.org/10.1515/geo-2020-0204

NASA Goddard Space Flight Center, Ocean Biology Processing Group. (2022a) *Chlorophyll a (chlor_a) [Dataset]*. NASA OB.DAAC. Retrieved from https://oceancolor.gsfc.nasa.gov/resources/atbd/chlor_a/

NASA Goddard Space Flight Center, Ocean Biology Processing Group. (2022b). *Particulate organic carbon (POC) [Dataset]*. NASA OB.DAAC. Retrieved from https://oceancolor.gsfc.nasa.gov/resources/atbd/poc/

NASA Goddard Space Flight Center, Ocean Biology Processing Group (2022c). *MODIS/AQUA ocean color reprocessing 2022.0 [WWW Document]*. NASA OB.DAAC. Retrieved from https://oceancolor.gsfc.nasa.gov/data/reprocessing/r2022/aqua/

National Academies of Sciences, Engineering, and Medicine. (2022). *A research strategy for ocean-based carbon dioxide removal and sequestration, A research strategy for ocean-based carbon dioxide removal and sequestration*. The National Academies Press. https://doi.org/10.17226/26278

Olgun, N., Duggen, S., Andronico, D., Kutterolf, S., Croot, P. L., Giammanco, S., et al. (2013). Possible impacts of volcanic ash emissions of Mount Etna on the primary productivity in the oligotrophic Mediterranean Sea: Results from nutrient-release experiments in seawater. *Marine Chemistry*, *152*, 32–42. https://doi.org/10.1016/j.marchem.2013.04.004

Ossaka, J. (1974). On the activity and development of volcano Nishinoshima, Bonin Islands. *Journal of Geography (Chigaku Zasshi)*, *83*(2), 125–133. (in Japanese). https://doi.org/10.5026/jgeography.83.2_125

Ossaka, J., Adachi, N., Tsuchide, M., & Nogami, K. (2000). Chemical compositions of discolored sea water around Izu-Oshima at the 1986 eruption. *Bulletin of the Volcanological Society of Japan*, *45*(5), 271–280. (in Japanese). https://doi.org/10.18940/kazan.45.5_271

Prata, A. J. (2009). Satellite detection of hazardous volcanic clouds and the risk to global air traffic. *Natural Hazards*, *51*(2), 303–324. https://doi.org/10.1007/s11069-008-9273-z

Pulido-Villena, E., Rrolle, V., & Guieu, C. (2010). Transient fertilizing effect of dust in P-deficient LNLC surface ocean. *Geophysical Research Letters*, *37*(1), L01603. https://doi.org/10.1029/2009GL041415

Redfield, A. C. (1934). On the proportions of organic derivatives in sea water and their relation to the composition of plankton. *James Johnstone Memorial*, 176–192.

Redfield, A. C. (1958). The biological control of chemical factors in the environment. *American Scientist*, *46*, 205–221.

Rousseaux, C. S. G., Lowe, R., Feng, M., Waite, A. M., & Thompson, P. A. (2012). The role of the Leeuwin Current and mixed layer depth on the autumn phytoplankton bloom off Ningaloo Reef, Western Australia. *Continental Shelf Research*, *32*, 22–35. https://doi.org/10.1016/j.csr.2011.10.010

Shinohara, M., Ichihara, M., Sakai, S., Yamada, T., Takeo, M., Sugioka, H., et al. (2017). Continuous seismic monitoring of Nishinoshima volcano, Izu-Ogasawara, by using long-term ocean bottom seismometers. *Earth Planets and Space*, *69*(1), 159. https://doi.org/10.1186/s40623-017-0747-7

Sigman, D. M., & Casciotti, K. L. (2001). Nitrogen isotopes in the ocean. *Encyclopedia of Ocean Sciences*, 1884–1894. https://doi.org/10.1006/rwos.2001.0172

Smetacek, V., Klaas, C., Strass, V. H., Assmy, P., Montresor, M., Cisewski, B., et al. (2012). Deep carbon export from a Southern Ocean iron-fertilized diatom bloom. *Nature*, *487*(7407), 313–319. https://doi.org/10.1038/nature11229

Steinmetz, F., Deschamps, P.-Y., & Ramon, D. (2011). Atmospheric correction in presence of sun glint: Application to MERIS. *Optics Express*, *19*(10), 9783–9800. https://doi.org/10.1364/oe.19.009783

Tagliabue, A., Twining, B. S., Barrier, N., Maury, O., Berger, M., & Bopp, L. (2023). Ocean iron fertilization may amplify climate change pressures on marine animal biomass for limited climate benefit. *Global Change Biology*, *29*(18), 5250–5260. https://doi.org/10.1111/gcb.16854

Tamura, Y., Ishizuka, O., Sato, T., & Nichols, A. R. L. (2019). Nishinoshima volcano in the Ogasawara Arc: New continent from the ocean? *Island Arc*, *28*, e12285. https://doi.org/10.1111/iar.12285

Tramontano, S., Gualda, G. A. R., & Ghiorso, M. S. (2017). Internal triggering of volcanic eruptions: Tracking overpressure regimes for giant magma bodies. *Earth and Planetary Science Letters*, *472*, 142–151. https://doi.org/10.1016/j.epsl.2017.05.014

Volk, T., & Hoffert, M. I. (1985). Ocean carbon pumps: Analysis of relative strengths and efficiencies in ocean-driven atmospheric CO_2 changes. In *The carbon cycle and atmospheric CO_2: Natural variations Archean to present*. In *Geophysical monograph series* (pp. 99–110). https://doi.org/10.1029/GM032p0099

Westberry, T. K., Behrenfeld, M. J., Shi, Y. R., Yu, H., Remer, L. A., & Bian, H. (2023). Atmospheric nourishment of global ocean ecosystems. *Science*, *380*(6644), 515–519. https://doi.org/10.1126/science.abq5252

Westberry, T. K., Shi, Y. R., Yu, H., Behrenfeld, M. J., & Remer, L. A. (2019). Satellite-detected ocean ecosystem response to volcanic eruptions in the subarctic Northeast Pacific Ocean. *Geophysical Research Letters*, *46*(20), 11270–11280. https://doi.org/10.1029/2019GL083977

Whiteside, A., Dupouy, C., Singh, A., Bani, P., Tan, J., & Frouin, R. (2023). Impact of ashes from the 2022 Tonga volcanic eruption on satellite ocean color signatures. *Frontiers in Marine Science*, *9*, 1028022. https://doi.org/10.3389/fmars.2022.1028022

Williams, D. B., & Ramsey, M. S. (2022). Analysis of ash emissions from the 2020 Nishinoshima eruption using ASTER thermal infrared orbital data. *Journal of Volcanology and Geothermal Research*, *421*, 107424. https://doi.org/10.1016/j.jvolgeores.2021.107424

Wilson, S. T., Hawco, N. J., Armbrust, E. V., Barone, B., Björkman, K. M., Boysen, A. K., et al. (2019). Kīlauea lava fuels phytoplankton bloom in the North Pacific Ocean. *Science*, *365*(6457), 1040–1044. https://doi.org/10.1126/science.aax4767

Wood, M., Hayes, C. T., & Paytan, A. (2023). Global quaternary carbonate burial: Proxy- and model-based reconstructions and persisting uncertainties. *Annual Review of Marine Science*, *15*(1), 277–302. https://doi.org/10.1146/annurev-marine-031122-031137

Wyatt, N. J., Birchill, A., Ussher, S., Milne, A., Bouman, H. A., Troein, E. S., et al. (2023). Phytoplankton responses to dust addition in the Fe-Mn co-limited eastern Pacific sub-Antarctic differ by source region. *Proceedings of the National Academy of Sciences of the United States of America*, *120*(28), e2220111120. https://doi.org/10.1073/pnas.2220111120

Xu, W., Wang, G., Cheng, X., Jiang, L., Zhou, W., & Cao, W. (2022). Characteristics of subsurface chlorophyll maxima during the boreal summer in the South China Sea with respect to environmental properties. *Science of the Total Environment*, *820*, 153243. https://doi.org/10.1016/j.scitotenv.2022.153243

Yacobi, Y. Z., & Zohary, T. (2010). Carbon:Chlorophyll a ratio, assimilation numbers and turnover times of Lake Kinneret phytoplankton. *Hydrobiologia*, *639*(1), 185–196. https://doi.org/10.1007/s10750-009-0023-3

Yanagisawa, H., Iino, H., Ando, S., Takagi, A., & Oikawa, T. (2020). Violent Strombolian Eruption from June to August 2020 of Nishinoshima Island, Ogasawara Islands, Japan. *Bulletin of the Volcanological Society of Japan*, *65*(4), 119–124. (in Japanese). https://doi.org/10.18940/kazan.65.4_119

Zhang, C., Yao, X., Chen, Y., Chu, Q., Yu, Y., Shi, J., & Gao, H. (2019). Variations in the phytoplankton community due to dust additions in eutrophication, LNLC and HNLC oceanic zones. *Science of the Total Environment*, *669*, 282–293. https://doi.org/10.1016/j.scitotenv.2019.02.068

References From the Supporting Information

Ackerman, S. A., Schreiner, A. J., Schmit, T. J., Woolf, H. M., Li, J., & Pavolonis, M. (2008). Using the GOES Sounder to monitor upper level SO_2 from volcanic eruptions. *Journal of Geophysical Research*, *113*, D14S11. https://doi.org/10.1029/2007jd009622

Crameri, F., Shephard, G. E., & Heron, P. J. (2020). The misuse of color in science communication. *Nature Communications*, *11*, 5444. https://doi.org/10.1038/s41467-020-19160-7

Nuñez, J. R., Anderton, C. R., & Renslow, R. S. (2018). Optimizing colormaps with consideration for color vision deficiency to enable accurate interpretation of scientific data. *PLoS One*, *13*(7), e0199239. https://doi.org/10.1371/journal.pone.0199239

Prata, A. J., Carn, S. A., Stohl, A., & Kerkmann, J. (2007). Long range transport and fate of a stratospheric volcanic cloud from Soufrière Hills volcano, Montserrat. *Atmospheric Chemistry and Physics*, *7*(19), 5093–5103. https://doi.org/10.5194/acp-7-5093-2007

Sears, T. M., Thomas, G. E., Carboni, E., Smith, A. J. A., & Grainger, R. G. (2013). SO_2 as a possible proxy for volcanic ash in aviation hazard avoidance. *Journal of Geophysical Research: Atmospheres*, *118*(11), 5698–5709. https://doi.org/10.1002/jgrd.50505

Watson, I. M., Realmuto, V. J., Rose, W. I., Prata, A. J., Bluth, G. J. S., Gu, Y., et al. (2004). Thermal infrared remote sensing of volcanic emissions using the moderate resolution imaging spectroradiometer. *Journal of Volcanology and Geothermal Research*, *135*(1–2), 75–89. https://doi.org/10.1016/j.jvolgeores.2003.12.017